1-1-2017

Beneficial Tensile Mean Strain Effects on the Fatigue Behavior of Superelastic NiTi

Benjamin Andrew Rutherford

Beneficial tensile mean strain effects on the fatigue behavior of superelastic NiTi

By

Ben Andrew Rutherford

A Thesis
Submitted to the Faculty of
Mississippi State University
in Partial Fulfillment of the Requirements
for the Degree of Master of Science
in Mechanical Engineering
in the Department of Mechanical Engineering

Mississippi State, Mississippi

May 2017

Beneficial tensile mean strain effects on the fatigue behavior of superelastic NiTi

By

Ben Andrew Rutherford

Approved:

_____

Tonya W. Stone
(Major Professor)

_____

Nima Shamsaei
(Director of Thesis / Committee Member)

_____

Matthew W. Priddy
(Committee Member)

_____

Yucheng Liu
(Graduate Coordinator)

_____

Jason M. Keith
Dean
Bagley College of Engineering

Name: Ben Andrew Rutherford

Date of Degree: May 5, 2017

Institution: Mississippi State University

Major Field: Mechanical Engineering

Major Professor: Dr. Tonya W. Stone

Title of Study: Beneficial tensile mean strain effects on the fatigue behavior of superelastic NiTi

Pages in Study 76

Candidate for Degree of Master of Science

In this work, beneficial effects of tensile mean strain on fatigue behavior and microstructure of superelastic NiTi (i.e. Nitinol) are studied. Most applications, such as endovascular stents made with NiTi, are subjected to a combination of constant and cyclic loading; thus, understanding the fatigue behavior of NiTi undergoing mean strain loading is necessary. Cyclic strain-controlled fatigue tests are designed to investigate the effects of tensile mean strain on fatigue of superelastic NiTi. Experimental observations show that combinations of large tensile mean strains and small strain amplitudes improve the fatigue life of superelastic NiTi. This behavior arises from reversible, stress-induced phase transformations. The phase transformations cause "stress plateaus" or strain ranges with no change in stress value. Scanning electron microscopy (SEM) of the fracture surfaces of specimens revealed generally short crack growth. Electron backscatter diffraction (EBSD) found the amount of residual martensite to be about ~8%, regardless of loading conditions

Keywords: NiTi, mean strain, SEM, superelasticity

DEDICATION

I would like to dedicate this research to my parents, Robert and Debbie Rutherford, to my brother, Austin, my two sisters, Cindi and Kelli, and my fiancé, Stephanie.

ACKNOWLEDGEMENTS

The author is grateful to the many people whose assistance tremendously influenced the completion of this Thesis. The first person I want to thank specifically is Dr. Shamsaei, my Thesis Director, for inspiring me to research fatigue as well as providing me the ability to do so while giving me direction on my research. The author also expresses appreciation to Dr. Daniewicz, who provided valuable knowledge and resources that aided in my research endeavors. Gratitude is also due to Dr. Stone, my Major Professor, and Dr. Priddy, my committee member. Finally, a special thanks to the Center for Advanced Vehicular Systems for allowing the use of testing equipment and other facilities that made this research possible.

TABLE OF CONTENTS

LIST OF TABLES

LIST OF FIGURES

NOMENCLATURE

A_f	Austenite finish temperature – the temperature at or above which the material is completely transformed to austenite
A_s	Austenite start temperature – the temperature at which upon heating the material begins to freely transform to austenite
A → M	Austenite to Martensite
ε_f^{AM}	A→M finish strain (i.e. the strain at which austenitic NiTi begins to transform into martensite)
ε_s^{AM}	A→M start strain (i.e. the strain at which austenitic NiTi has completely transformed into martensite)
σ_f^{AM}	A→M finish stress (i.e. the stress at which , upon loading, austenitic NiTi begins to transform into martensite)
σ_s^{AM}	A→M start stress (i.e. the stress at which, upon loading, austenitic NiTi has completely transformed into martensite)
M_f	Martensite finish temperature – the temperature at or below which the material is completely transformed to martensite
M_s	Martensite start temperature – the temperature at which upon cooling the material begins to freely transform to martensite
M → A	Martensite to Austenite
ε_f^{MA}	M→A finish strain (i.e. the strain at which austenitic NiTi begins to transform into martensite)
ε_s^{MA}	M→A start strain (i.e. the strain at which austenitic NiTi has completely transformed into martensite)
σ_f^{MA}	M→A finish stress (i.e. the stress at which , upon loading, austenitic NiTi begins to transform into martensite)

σ_s^{MA}	M→A start stress (i.e. the stress at which, upon loading, austenitic NiTi has completely transformed into martensite)
ε_{max}	Maximum strain
σ_{max}	Maximum stress
ε_m	Mean strain (i.e. average strain)
σ_m	Mean stress (i.e. average stress)
ε_{min}	Minimum strain
σ_{min}	Minimum stress
N_f	Number of cycles to failure
$2N_f$	Number of reversals to failure
ε_a	Strain amplitude (i.e. alternating strain)
R_ε	Strain ratio of a cyclic loading (ε_{min} / ε_{max})
σ_a	Stress amplitude (i.e. alternating stress in a cyclic test)
R_σ	Stress ratio of a cyclic loading (σ_{min} / σ_{max})

CHAPTER I

INTRODUCTION

NiTi, also referred to as Nitinol, is a nearly equiatomic alloy of nickel, Ni, and titanium, Ti. The unique properties of NiTi were first discovered at the Naval Ordinance Laboratory by Buehler and Wang in 1962 (Buehler et al., 1963). These properties, which will be further discussed later, made the material popular for applications that are otherwise impossible for most other material systems, such as self-expanding endovascular stents.

Background

After the discovery of NiTi's properties of superelasticity and shape memory, the use of shape memory alloys (SMA) has gradually increased. An SMA is a material system that can be programmed to "remember" an undeformed shape after seemingly permanent deformation has been applied. NiTi was important to the expansion of SMA applications since it additionally possessed properties such as excellent wear resistance, high corrosion resistance, relatively high ductility for SMA's, and biocompatibility (Mahtabi et al., 2015a). Initially used in the aerospace industry for actuators in military aircraft, NiTi gradually expanded to other industrial applications such as biomedical (Duerig et al., 1999; Pelton et al., 2008; Shabalovskaya, 1996), automotive (Duerig et al., 2013; Leo et al., 1998; Mohd Jani et al., 2014), as well as other uses, including as eyeglass frames (Kauffman and Mayo, 1997). One of the drawbacks of NiTi is the cost

of manufacturing the material, which is generally produced through a process of vacuum induction melting. However, the recent development of additive manufacturing could help alleviate the cost of NiTi as it is cheaper to produce using this manufacturing technique. NiTi components printed in an additive manufacturing device also require less post-processing to create functional parts.

Superelasticity and Shape Memory

The key properties NiTi exhibits that make it desirable for numerous applications over cheaper, more easily manufactured materials are superelasticity and shape memory. These properties are linked to a reversible thermo-mechanical phase transformation in the material. Multiple microstructural phases exist in NiTi, but two specific phases tend to dominate the material matrix. A high temperature phase, also known as the parent phase, referred to as austenite and a low temperature phase, or daughter phase, referred to as martensite. The austenitic phase has a B2 crystal lattice type, which is similar to a BCC structure with a different center atom than the atoms on the corners (Otsuka and Ren, 2005). The martensitic phase has a B19' crystal lattice type, which is a primitive monoclinic unit cell (Otsuka and Ren, 2005). In NiTi research there are four characteristic temperatures used to describe its microstructure. These temperatures are, in order of hottest to coldest: A_f, at or above this temperature the material is fully austenite; A_s, when heating the temperature at which the material freely transforms to austenite; M_s, when cooling the temperature at which the material freely transforms to martensite; and M_f, at or below this temperature the material is fully martensite. In addition to temperature, austenite can be transformed into martensite by strain energy

distortion due to increased mechanical loading. This sets the framework for explaining the mechanism behind superelasticity and shape memory.

Superelasticity is a phenomenon experienced by NiTi, and other SMA's, when the material matrix is in the austenitic phase with the temperature T greater than or equal to A_f. When deformation is applied to the sample under this condition such that the material undergoes an apparent yielding. However, plastic flow has not occurred, rather stress-induced phase transformation is initiated. The stress and strain corresponding to this point on the stress-strain curve are called A → M start stress (σ_s^{AM}) and A → M start strain (ε_s^{AM}), respectively. The stress is nearly constant for the next region on the stress-strain curve for a range of strains (2.5 – 10%). This region is referred to as the stress plateau or phase transformation plateau. The end of the plateau is denoted by the point on the curve where the stress is the A → M finish stress (σ_f^{AM}) and the strain is the A → M finish strain (ε_f^{AM}). If deformation continues after that point, the material has a linear elastic response with a primarily martensitic microstructure. The material may then be unloaded which will cause the stress-strain response to follow the slope of the linear elastic martensitic region until it reaches an unloading stress plateau. This stress level is generally lower in magnitude than the loading stress plateau and begins at the M → A start stress (σ_s^{MA}) and M → A start strain (ε_s^{MA}). The unloading stress plateau behaves similarly to the loading stress plateau until it reaches the austenitic linear elastic region. This point is denoted by the M → A finish stress (σ_f^{MA}) and M → A finish strain (ε_f^{MA}). The stress-strain curve then follows the initial slope of the austenitic linear elastic region back to the strain axis. A diagram of this behavior is shown in Figure 1 The shape of the

hysteresis loop caused by this mechanical response is generally described as "flag shaped".

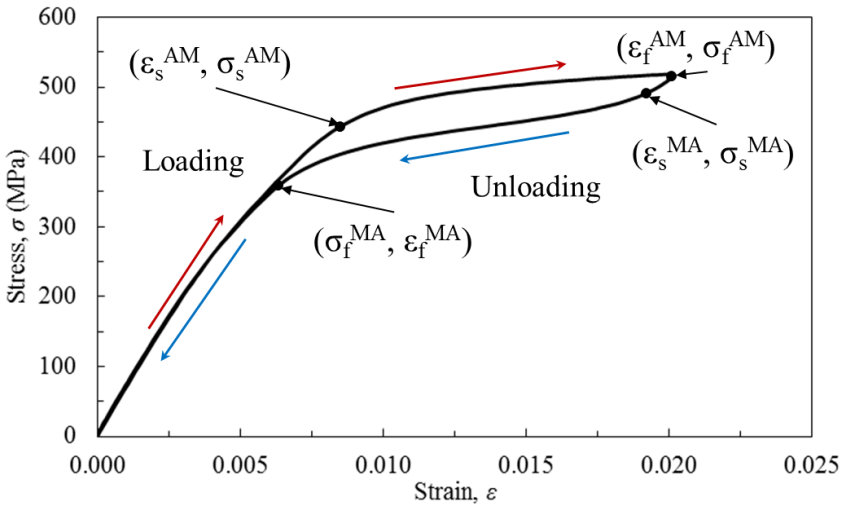

Figure 1 Schematic of superelastic stress-strain response

Shape memory behavior is similar to that of superelasticity, but incorporates temperature to recover seemingly plastic strains. If the sample is held at a temperature between the A_s and M_s temperatures and deformed, the mechanical response will be different from superelasticity. The material must also be austenitic at the start of deformation. The shape-memory material undergoes typical elastic-plastic stress-strain behavior when deformation is applied. It will follow an elastic slope until an apparent yield where the stress becomes constant over a range of strain. However, once the deformation is unloaded, it will unload on a linear path that is parallel to the linear elastic region. This is due to the lack of thermal energy to trigger reverse transformation ($T < A_s$), which leads to retained martensite and the residual strain thereof. If heat is then

added such that the material's temperature exceeds the A_f temperature, then the material will convert to austenite, recover the residual strain, and "remember" the original shape. This response can be plotted thermo-mechanically as seen in Figure 2

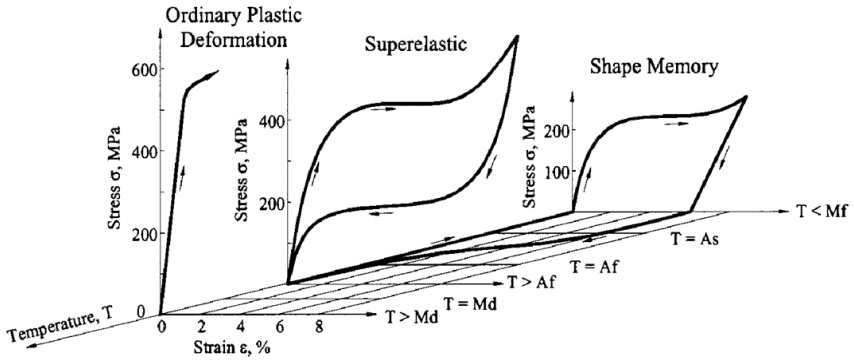

Figure 2 Diagram of the stress-strain response of NiTi under non-transforming, superelastic, and shape memory conditions (DesRoches et al., 2004)

For the sake of completeness it is also worth talking about another characteristic temperature, M_d, which is the hottest characteristic temperature. This is the temperature at or above which the material no longer exhibits any phase transformation. The internal energy of the material at this temperature is so high that it is no longer energetically favorable for martensite to form as a result of distortional strain energy. The mechanical response of this material, stable austenite, is similar to brittle materials. It has a linear elastic portion that experiences yield, followed by fracture, with relatively little strain after yielding.

The importance of these properties to NiTi cannot be overstated as its popularity in the biomedical field is more or less completely dependent on them. The push to get more minimally invasive in surgery has led to the need for components that can function

even after undergoing incredibly high strains. Some examples of such devices are the Homer Mammalok (Duerig et al., 1999; Pelton et al., 2004) as well as the atrial septal defect occlusion system (ASDOS) (Duerig et al., 1999). That said, superelastic materials, especially ductile ones, lend themselves well to that sort of design. Likewise, shape memory can be easily exploited to create thermally regulated actuators in the automotive and aerospace industry.

Motivation and Objective

As with material systems that are designed for use in various applications, components made of NiTi must be designed to perform a function as designed and without unexpected, sudden failure, e.g. fracture, severe deformation, and buckling. In order reduce the chance of component failure the material behavior must be thoroughly understood, tested, and validated. Among these behavioral properties to be understood are those of fatigue for applications undergoing cyclic loading. Fatigue can occur in many different modes, from constant amplitude, fully reversed, uniaxial loading up to variable amplitude, out-of-phase, multi-axial loading.

In this work the mode being investigated is the case of constant amplitude, uniaxial, tensile mean strain cyclic loads. This type was chosen to test the reports of the beneficial effects of tensile mean strains on fatigue behavior of NiTi. This type of loading is a simplified version of the loading that may be seen by some NiTi devices, such as endovascular stents. An endovascular NiTi stent is designed such that there is a compressive interference fit with the wall of the blood vessel (mean strain) that also experiences the periodic pressure wave of the pulse from the heartbeat (cyclic strain).

For this reason, it is vital to know the fatigue behavior of NiTi to reduce the risk of component failure that leads to increased costs, injury, and possibly loss of life.

The research was carried out on cylindrical NiTi specimen with a uniform gage section under strain-controlled loading. The stress-strain data generated by these tests, as well as microstructural analysis of the specimens after failure, was examined to establish a link between the fatigue properties and microstructure of superelastic NiTi. A model was then implemented to investigate whether it can account for the fatigue behavior of superelastic NiTi under tensile mean strain.

Organization of the Work

This work has been organized in the following manner. Chapter II provides literature review on the current state of research on the topic of NiTi fatigue. Following the literature review, the next chapter outlines the experimental setup for the testing and reason for the experimental design is discussed. In Chapter IV the results from the experimentation and a discussion of the active mechanisms using various post-processing techniques as well as information from the literature on the material behavior. In Chapter V a summary of the significant findings from this research is presented along with a concise conclusion of the work. Finally, a recommendation of future works on fatigue of NiTi is provided. References are documented at the end of the thesis.

CHAPTER II

LITERATURE REVIEW

NiTi and the unique properties it possesses were discovered and examined in the early 1960's by Buehler et al. (Buehler et al., 1963). The unique effect of the microstructure and phase transformation on the stress-strain response makes the material novel and presents new challenges in fatigue modelling. To understand this material's mechanical response there is a lot of microstructural phenomena to understand. This section of the work serves to provide some background from the research literature on the mechanism and behavior of NiTi. Specifically, this section covers academic literature on the nature of microstructure and fatigue behavior.

Before discussing the literature on microstructural properties and fatigue characteristics of NiTi alloys it is important to remember why it matters. NiTi alloys are currently used or planning to be used in numerous industrial applications. In the Biomedical Industry NiTi is used in vena cava filters (Duerig et al., 1999), Homer Mammalok devices (Pelton et al., 2004), endodontic files (Bahia and Buono, 2005; Condorelli et al., 2010), and arterial stents (Allie et al.; Nikanorov et al., 2008). Also in biomedical applications, additively manufactured (AM) NiTi is being used to make patient specific implants (Elahinia et al., 2012; Shayesteh Moghaddam et al., 2016). The Aerospace Industry started using NiTi alloys as actuators and that has continued to be the primary application of NiTi (Casati et al., 2011; Elahinia, 2015; Fumagalli et al., 2009;

Mertmann and Vergani, 2008). More recently civil applications have emerged for NiTi alloys including seismic dampers for buildings (DesRoches et al., 2004) as well as structural braces (Song et al., 2006). These applications will all experience cyclic load, and in many cases the failure of a component can result in death at worst and severe discomfort at best.

Overview of NiTi Microstructure

In 2005, Otsuka and Ren (Otsuka and Ren, 2005) conducted a literature review of the metallurgical aspects of NiTi alloys. Points of interest to this work discussed in their study (Otsuka and Ren, 2005) pertain to characterization of various phases of NiTi, microstructure mechanisms involved in phase transformation, and understanding the phase diagram. With that said, the best place to start is in the phase diagram shown in Figure 3.

The primary region of interest in the phase diagram is the region which forms the austenitic phase of NiTi alloys. This occurs when the appropriate temperature and atomic/weight percentages of each element are combined. For NiTi this occurs within the bounds at 48 to 56 at. % Nickel at a temperature range of 630 to 1310˚C. It is also worth noting that above 1090˚C of an order – disorder transition to BCC exists, but has not been confirmed by other works (Otsuka and Ren, 2005). If the elements are mixed and heated in this region and cooled to room temperature, whether by air cooling or quenching, the B2 austenite phase structure will be preserved. Another important region is the Ti_3Ni_4 region. This region is located next to the NiTi region within the dashed box, bounded by 50 to 57 atomic percent Nickel and temperatures ranging from 630 to 1118˚C. The Ti_3Ni_4 phase makes up precipitates in the material matrix that can be

induced by heat treatments (Gall et al., 1999a, 2001). Ti_3Ni_4 precipitates in the material matrix help to serve as local areas of preferential martensite formation in the material matrix (Gall et al., 1999a). The stress contours surrounding the precipitate aid in developing martensitic variants better suited to the applied load.

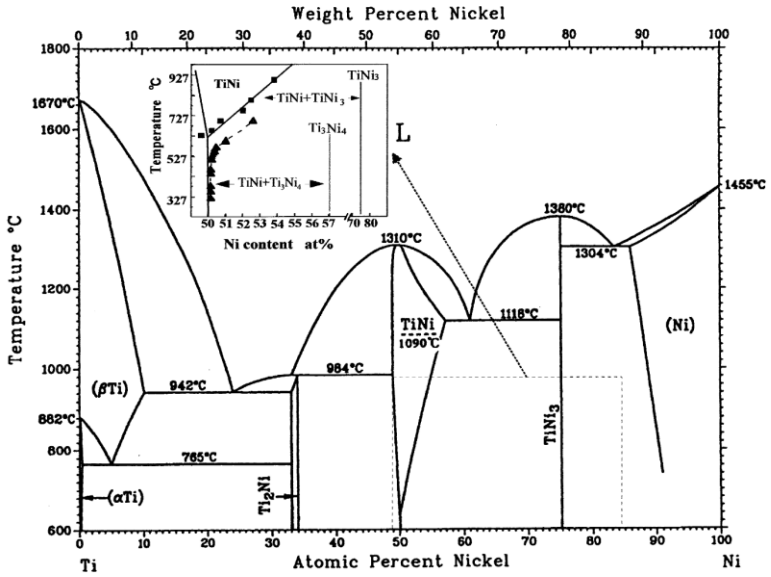

Figure 3 Phase diagram of binary NiTi alloys (Otsuka and Ren, 2005)

As mentioned previously, the austenite phase of NiTi has a B2 (CsCl) crystal structure. This structure is extremely similar to the BCC lattice with the notable exception that the atom in the center is different from the atoms on the corners in B2. The basic schematic austenitic NiTi can be seen in Figure 4. The primary slip system for superelastic NiTi has been reported to be {011}<100> (Norfleet et al., 2009; Pelton, 2011). The lattice parameter of the austenite phase of NiTi has been reported as 0.3015 nm (Otsuka and Ren, 2005).

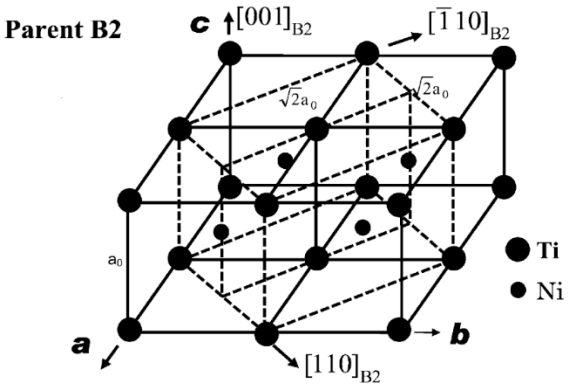

Figure 4 Schematic of four austenite, B2, unit cells of NiTi (Otsuka and Ren, 2005)

The other primary phase for consideration in this work is the martensitic phase of NiTi. Also mentioned in the introduction is the lattice type for the martensitic variants of NiTi, B19'. This unit cell type is a primitive monoclinic type, which has one of the most complex unit cell structures possible, with the exception of triclinic and non-primitive monoclinic types. Unlike cubic lattice structures, monoclinic lattice structures have four independent lattice parameters: a unique distance on each axis as well as a skewed axis (not perpendicular). The shape resembles a leaning rectangle and can be seen in Figure 5. The lattice parameters of the B19' phase of NiTi were reported as a= 0.2885 nm, b= 0.4120 nm, c= 0.4622 nm, and β= 96.8˚ (Michal and Sinclair, 1981). The formation of martensite sometimes goes through intermediate phase transformations, such as R (Rhombohedral phase) and B19 (orthorhombic martensite phase), but those phases are typically fully consumed without ever having a majority volume fraction (Otsuka and Ren, 2005). Due to the low symmetry associated with the monoclinic lattice there are 24 different variants, i.e. orientations, of martensite in NiTi that come in twinned pairs (Gall et al., 1999a).

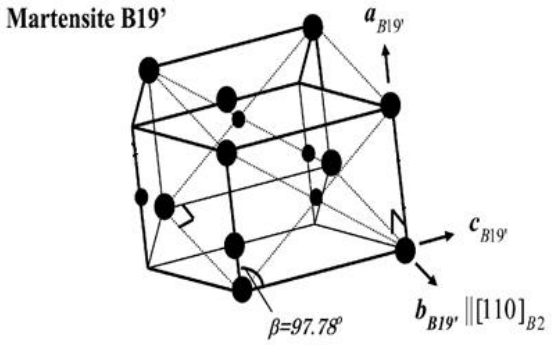

Figure 5 Schematic of two martensite, B19', unit cells of NiTi, modified from Otsuka and Ren (Otsuka and Ren, 2005)

Heat treatments and other thermo-mechanical processes affect the mechanical properties of NiTi as is typical for most metallic materials (Dieter, 1961). However, due to the microstructural influence on the mechanical response of NiTi processing conditions can create complex interactions. Aging has been shown to vary the size and morphology of Ti_3Ni_4 precipitates (Gall et al., 1999a). Precipitations were shown to affect the stability and evolution of the phase transformation's mechanical response (Gall et al., 1999a). This information agrees with another study (Sehitoglu et al., 2001) in single-crystal behavior of NiTi. Additionally, Sehitoglu et al. also reported that peak-aging with very fine precipitate structure improves the fatigue behavior for both austenite and martensite. Therefore, the parameters of the material processing technique must be judiciously considered in order to acquire the desired properties and material behavior.

The texture of martensitic NiTi was found to change slightly under repeated heating and cooling (Benafan et al., 2014). This shift in texture is attributed to the

material preferentially transforming to accommodate the internal strain associated with thermal expansion. The texture of the austenitic phase was found to remain relatively unchanged, which makes sense due to the high level of symmetry it possesses. On the other hand the austenite experienced an increase in lattice defects with increasing cycles related to phase transformation (Benafan et al., 2014).

Under tensile loading, Delville et al. (Delville et al., 2011) found that dislocation density increases with increasing grain size. They also speculate that dislocations associated with superelastic cycling result in local plasticity, which corroborates the findings of others studies (Delville et al., 2011; Gall et al., 1999a; Iadicola and Shaw, 2002; Norfleet et al., 2009). The study (Delville et al., 2011) found that macroscopic behavior reflects the accumulation of dislocation defects in the degradation of the stress-strain properties with cyclic loading. Delville et al. points out the existence of deformation twins in the austenitic structure that are retained after forward and reverse phase transformation. This finding indicates an additional deformation mechanism present in NiTi alloys.

In a series of studies Frotscher et al. (Frotscher et al., 2009, 2011) investigated the microstructure of NiTi stents before, during, and after cyclic loading. They reported that the microstructure does not significantly change from fatigue testing (Frotscher et al., 2009). A minor amount of martensite is retained after testing, and that martensite is stabilized by plastic deformation (Frotscher et al., 2009). Similar to Delville's team (Delville et al., 2011) Frotscher and company (Frotscher et al., 2011) reported increased dislocation density with increased cycles in the superelastic regime. They (Frotscher et

al., 2011) also note that the increase is not homogeneous, and that some regions in the specimens see an increase where others do not.

In a study on the cyclic stress-strain response of NiTi Mao et al. (Mao et al., 2006) reported microstructural influences played a key role. Due to textural evolution of the specimens under repeated loading the phase transformation start stress, σ_s^{AM} is reduced (Mao et al., 2006). The material re-orients the grains to remove low-angle grain boundaries that in turn raises the Schmid factor. They (Mao et al., 2006) also found that the microstructural re-orientation stabilizes after 10 cycles.

The phase transformation stresses, i.e. σ_s^{AM} and σ_s^{MA}, similar to the yield stress, ultimate tensile stress, and ductility are affected by material processing (Frick et al., 2005; Gall et al., 1999a; Pelton et al., 2000). Pelton and co-workers (Pelton et al., 2000) performed a study on the effect of aging treatment and test temperature on the mechanical properties of NiTi wires. They found that the austenite finish temperature, A_f varied from about 5˚C to 61˚C with changes in aging temperature and time (Pelton et al., 2000). Another study (Gall et al., 1999b) found that the M_s temperature for peak-aged and over-aged samples was higher than that of solutionized NiTi. This was attributed to the local stress concentrations in peak-aged samples and Ni depletion in the over-aged specimens (Gall et al., 1999b). The driving mechanism behind this behavior was determined to be a product of two metallurgical phenomena. The first is the rate of precipitation nucleation, and the second is the rate of precipitation diffusion. The nucleation rates increased with decreased aging temperature, while the diffusion rates increased with increased aging temperature (Pelton et al., 2000). For this reason the intermediate aging temperatures, 350˚C to 450˚C had the greatest effect on A_f over the first hour of aging (Pelton et al.,

2000). Beyond an hour the rate of diffusion precipitation overpowered the nucleation rates influence resulting in higher temperatures, i.e. 550˚C (Pelton et al., 2000).

The importance of the effect of aging treatments on the A_f temperature comes from the influence of the mechanical response. All the characteristic temperatures are simultaneously affected by aging, and the general approximation between the A_f temperature and the M_s temperature is given by $A_f = 40^{\circ}C + M_s$ (Robertson et al., 2012). These characteristic temperatures indicate the mechanical response at a given test temperature, i.e. superelasticity or shape memory behavior. In the same study mentioned earlier, Pelton et al. (Pelton et al., 2000) investigated the effects of testing temperature on the mechanical response of NiTi wires with an initial $A_f = 11^{\circ}C$. They found that the phase transformation plateau stress, σ_s^{AM} increased with increasing test temperature (Pelton et al., 2000). In general, the yield and ultimate stress decrease with increasing test temperature (Dieter, 1961). In NiTi the same trend is seen for the ultimate tensile stress (Pelton et al., 2000). This behavior explains the existence of the M_d temperature. As seen in Figure 6. (Pelton et al., 2000) the σ_s^{AM}, referred to as "upper plateau stress" eventually becomes greater than the ultimate stress around 175˚C. At this point the austenite phase is energetically more stable because austenite and the thermal energy cannot be overcome by strain distortion energy before failure occurs.

Additionally, cold working and hot rolling processes for strengthening a material, e.g. increasing the yield strength, was investigated on NiTi by Gall and co-workers (Gall et al., 2008). In their study (Gall et al., 2008) it was concluded that the strengthening processes also improved the cyclic stability of low-cycle fatigue. It was also reported that the hot-rolled material had similar fracture toughness to superelastic NiTi, regardless

of aging treatment, found in the literature (Gall et al., 2008). However, the cold-drawn material had a fracture threshold value approximately 80% weaker than the hot-rolled (Gall et al., 2008). That makes cold-drawn NiTi extremely brittle. The fracture threshold of NiTi was lower than some ceramics and 2 to 25 times lower than any other metallic material (Gall et al., 2008).

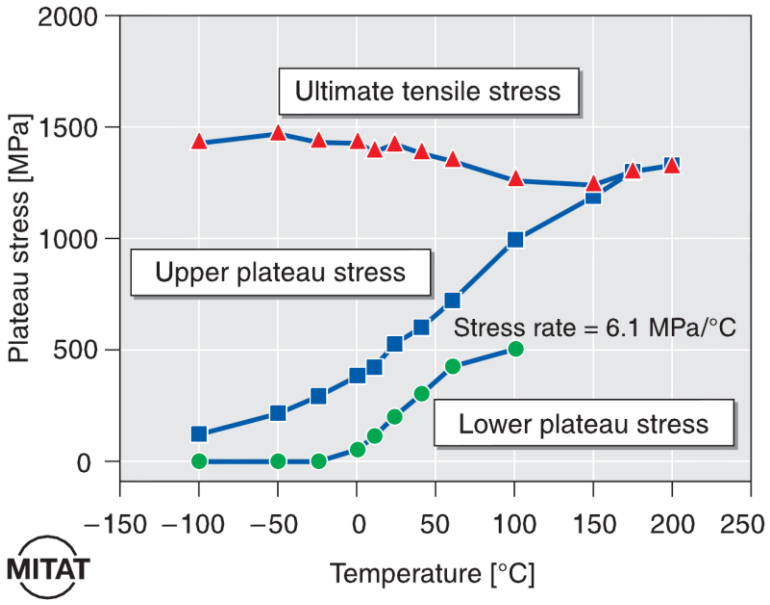

Figure 6 Effect of test temperature on ultimate tensile stress, upper plateau stress, and lower plateau stress (Pelton et al., 2000)

Overview of NiTi Fatigue

The earliest systematic fatigue studies in stress-life, strain-life, and fatigue crack growth behavior of NiTi alloys were carried out by Melton and Mercier (Melton and Mercier, 1979b, 1979a) in the late 1970's. More recently, some of their conclusions have been questioned, since the quality of the specimens' chemical compositions may have had an effect on the research (Mahtabi et al., 2015a; Robertson et al., 2012). Despite the

conclusions, the experimental observations into the mechanical behavior are still relevant now. After Melton and Mercier, the next thorough fatigue study came from Miyazaki and associates (Miyazaki et al., 1986). Since then, there have been many fatigue studies on NiTi under various loading conditions. They are summarized in (Robertson et al., 2012) and (Mahtabi et al., 2015a).

Melton and Mercier (Melton and Mercier, 1979a) provided insight into the general fatigue behavior of NiTi under both force-controlled (stress-based) and displacement-controlled (strain-based) conditions. Under stress-based testing, superelastic NiTi performed better than the mixed-phase, material consisting of both austenite and martensite, and thermally martensitic NiTi (Melton and Mercier, 1979b). Under strain-based testing (Melton and Mercier, 1979b, 1979a) found the opposite trend, namely that superelastic NiTi performed the worst, with mixed-phase performing better and thermally martensitic NiTi performing the best. In addition to those findings, Melton and Mercier (Melton and Mercier, 1979b) observed rapid cyclic hardening early in the fatigue life, i.e. first 10 cycles, and a narrowing of the hysteresis loop throughout the life of the test specimen.

The narrowing of the hysteresis loop is related to microstructural changes according to Eggeler et al. (Eggeler et al., 2004). The microstructure was found to control both the stability of the hysteresis as well as the localized transformation. The degradation of the stress-strain properties with cyclic loading is associated with plasticity, which is attributed to incomplete reverse transformation during testing (Eggeler et al., 2004). The study (Eggeler et al., 2004) additionally reported the fatigue damage to be governed by crack initiation. Another study (Scirè Mammano and Dragoni, 2014) into

the functional fatigue of NiTi found several trends. The σ_a versus N_f plot exhibited tri-linear behavior. The ε_a versus N_f plot exhibited linear monotonously decreasing behavior with no fatigue limit. The σ_a versus N_f data in which the ε drift was limited experienced a higher endurance limit (Scirè Mammano and Dragoni, 2014).

Miyazaki and co-workers (Miyazaki et al., 1986) reported the same relatively poor performance of superelastic NiTi under strain-life methodology as Melton and Mercier. Miyazaki et al. (Miyazaki et al., 1986) also conducted pulsating fatigue testes ($R_\sigma = 0$) in the stress-life method and found the same trend as in the stress-life data as Melton and Mercier did for fully-reversed tests ($R_\sigma = -1$).

Several studies (Kim, 2002; Miyazaki et al., 1999; Patel et al., 2007; Pelton et al., 2013; Sawaguchi et al., 2003; Tobushi et al., 1997, 1998) have been performed on the rotating bending fatigue behavior of superelastic NiTi. Kim (Kim, 2002) found that the phase transformation start stress, σ_s^{AM} increased with increasing Nickel content and that the ε_a versus N_f could be split into three linear segments regardless of Nickel content. Sawaguchi et al. (Sawaguchi et al., 2003) also reported the ε_a versus N_f behavior to have three distinct linear regions. They (Sawaguchi et al., 2003) examined fracture surfaces and suggested that the first region's crack growth is driven by surface flaws. The second region's crack initiation was dictated by stress concentrations in the material matrix. Miyazaki and company reported a multi-linear ε_a versus N_f behavior as well (Miyazaki et al., 1999). Both Kim (Kim, 2002), the Miyazaki group (Miyazaki et al., 1999), the Pelton group (Pelton et al., 2013), and the Tobushi group (Tobushi et al., 1997) all found increased testing temperature led to decreased fatigue lives. Pelton and co-workers also

reported a quad-linear ε_a versus N_f behavior (Pelton et al., 2013). Each region of the Pelton group's ε_a versus N_f plot correlated to a characteristic phase of the material.

Under thermal fatigue, done by heating/cooling cycles, the characteristic temperatures are reported to shift (He et al., 2006). The shift in the temperatures occurs during the stabilization of the material within the first ten cycles. The M_f, M_s, and A_f temperatures all decreased while the A_s temperature increased (He et al., 2006). The study does not speculate as to what causes this phenomenon or whether it may occur in mechanically-based fatigue testing. Urbina et al. (Urbina et al., 2009) also investigated thermally cycled NiTi. The findings from this study recommend thermally pre-loading at 0 stress NiTi if it will undergo R-phase transformation during service. Lagoudas et al. (Lagoudas et al., 2009) reported that under thermo-mechanical loading in the phase transformation regime that the residual strain in the specimens corresponded to the fatigue life. However, they (Lagoudas et al., 2009) did not see a multi-linear ε_a versus N_f since they did not do any testing in the linear elastic regime.

NiTi was tested under uniaxial tension-tension conditions in a study by Maletta et al. (Maletta et al., 2012). They reported the hysteresis loops degrades for approximately the first 100 cycles until it stabilizes. The degradation was also reported (Maletta et al., 2012) to be more drastic in nature with increased ε_a. Under torsional loading very few studies have been conducted (Moumni et al., 2009; Predki et al., 2006). Predki and company performed a preliminary test on the torsional fatigue properties of NiTi alloys. Under fully reversed loading conditions, they (Predki et al., 2006) reported a high sensitivity of damping capacity to frequency and increased cycles. Conversely, the

fatigue rupture that occurred appeared to minimally affected by the same two parameters (Predki et al., 2006).

Fatigue crack growth of NiTi was thoroughly examined in the early 2000's by McKelvey and Ritchie (McKelvey and Ritchie, 2001). In this study, the researchers (McKelvey and Ritchie, 2001) looked at the fatigue crack threshold and crack growth rates of four types of NiTi. Thermally stable austenite (tested above the M_d temperature), superelastic NiTi (tested above the A_f temperature), and two thermally martensitic NiTi (one below the M_f temperature and the other much lower than M_f). Of the materials tested, superelatic NiTi had the lowest fatigue crack threshold value, followed by thermally stable NiTi, and then both thermally martensitic NiTi (McKelvey and Ritchie, 2001). This result is significant for two reasons. First superelastic NiTi is the most commonly used, and second it demonstrates that the martensitic phase has superior fracture threshold properties. All four types exhibited similar crack growth rates (McKelvey and Ritchie, 2001). Another important finding was suppression of phase transformation at the crack tip. In-situ X-ray diffraction (XRD) revealed superelastic NiTi at the crack tip did not transform into martensite (McKelvey and Ritchie, 2001). This is attributed to the reason why superelastic NiTi does not have a comparable threshold value to martensite despite the applied stress being high enough to induce phase-transformation (McKelvey and Ritchie, 2001). The mechanism behind it is a tri-axial stress state due to the stress concentration at the crack tip (McKelvey and Ritchie, 2001). Since the stress concentration drastically increases for incredibly small radii, the poisson effect on the material induces stresses in the other axial directions. This leads to a reduction in distortion energy, which suppresses phase transformation.

Robertson and Ritchie also performed fatigue crack-growth and fracture toughness tests on stents made with NiTi. They (Robertson and Ritchie, 2007) reported similar threshold numbers to those of other studies (Gall et al., 2008; Gollerthan et al., 2009; McKelvey and Ritchie, 2001). Additionally, the crack-growth behavior had a dependency of the load ratio. The crack-growth data from the tests conducted in air were found to be not significantly different than those conducted in a saline solution to simulate body fluids (Robertson and Ritchie, 2007). This means that the corrosive effect experienced by NiTi in vitro does not greatly affect the fatigue performance of the device.

Similarly to McKelvey and Ritchie, Gollerthan et al. (Gollerthan et al., 2009) also performed a study on the fracture behavior of different phases of NiTi alloys. This study (Gollerthan et al., 2009) found that the P(Δ) curves for NiTi exhibit ductile behavior. However, NiTi does not undergo crack tip blunting as common with ductile materials (Gollerthan et al., 2009). This can be understood as a result of superelasticity. NiTi generally possesses a brittle nature with respect to fracture surface characteristics and stress-strain behavior in the M_d regime, seen in Figure 2 Since the material itself appears to be brittle with the exception of elongation, which is a result of superelasticity, crack tip blunting should not be expected. Lastly, Gollerthan et al. (Gollerthan et al., 2009) contend the claim of McKelvey and Ritchie (McKelvey and Ritchie, 2001) about transformation suppression at the crack tip. In situ synchrotron diffraction found martensitic formation ahead of the crack tip during testing (Gollerthan et al., 2009).

Holtz and associates (Holtz et al., 1999) also performed fracture tests on shape memory and superelastic NiTi. The reported characteristic temperatures were $M_f = 70^{\circ}C$,

M_s = 80 ˚C, A_s = 100 ˚C, and A_f = 120 ˚C (Holtz et al., 1999). The study reported an increase in the stress intensity threshold with increasing testing temperature starting at 30 ˚C. This behavior is contrary to the results of McKelvey and Ritchie's study in 2001 (McKelvey and Ritchie, 2001). However, this change can partially be attributed to the different chemical composition of NiTi that they (Holtz et al., 1999) used. The Holtz team used NiTi that was 49.9 at.% Nickel while the McKelvey study used 50.8 at.% Nickel, which is medical grade. NiTi alloys are very sensitive to chemical composition and this may explain the different threshold properties.

All the fatigue crack-growth studies mentioned thus far have reported uncharacteristically low fracture thresholds for NiTi as a metal. One study (Vaidyanathan et al., 2000) compared the fracture properties of pure NiTi to TiC particle reinforced composite NiTi. While the general fatigue crack-growth properties were found to be similar, they (Vaidyanathan et al., 2000) reported a slightly increased fracture threshold value for the reinforced composite samples. These findings can hopefully be used to find a beneficial reinforcement for NiTi components to extend the fatigue life. However, a study (Mahtabi et al., 2015b) on general fatigue behavior have found TiC to be a preferential initiation site for cracks in NiTi.

Mean Strain/Stress Fatigue and Modelling

Some of the earliest studies developed specifically to investigate the mean strain/stress behavior of NiTi occurred in the late 1990's and early 2000's (Morgan et al., 2004; Tabanli et al., 1999, 2001). These studies (Morgan et al., 2004; Tabanli et al., 1999, 2001) used the displacement-controlled (strain-based) methods and all found a peculiar result. The trend in fatigue behavior of NiTi under mean strain loading exhibited

non-monotonously decreasing fatigue life (Tabanli et al., 1999). This means that under certain mean strain loading conditions the fatigue life could actually improve, which is contrary to the general behavior of metals (Stephens et al., 2000). This concept has been probed using Finite-Element Analysis FEA in parallel with NiTi material properties to simulate fatigue life in several studies (Pelton et al., 2008; Tolomeo et al., 2000). More recently a study was carried out on the effects of mean strain on NiTi by varying R_ε (Mahtabi et al., 2015b). The findings from this study indicated a detrimental effect of tensile mean strains on the fatigue life of superelastic NiTi.

Tabanli and co-workers (Tabanli et al., 1999, 2001) conducted several studies on the effects of tensile mean strains on NiTi. The experiment implemented small strain amplitudes at various mean strain values to test NiTi with various microstructures (Tabanli et al., 1999). The different types are characterized by the phases present. One was completely austenitic, another was completely martensitic, and the rest were mixed phase with various volume fraction ratios of austenite to martensite (Tabanli et al., 1999, 2001). The results indicated that the fatigue life starts out high, then decreases to a relative minimum in a mixed phase with mostly austenite, and increases again into the fully martensitic region (Tabanli et al., 1999, 2001). The studies also include mean stress analysis for the tests, but this does not necessarily follow mean stress behavior under force-controlled (stress-based) testing techniques due to the stress plateau.

In 2004, Morgan and associates (Morgan et al., 2004) documented and reported the results of an experiment into mean strain testing of NiTi. They tested superelastic NiTi specimens with seven ε_a across three ε_m levels. The results showed a uniform increase in fatigue life for higher ε_m (Morgan et al., 2004). In the low cycle regime the

effects of the different ε_m were minimal, but at higher ε_m with lower ε_a the fatigue life vastly improved compared to ε_a at lower ε_m values (Morgan et al., 2004). The primary difference between Morgan et al.'s work and that of Tabanli et al.'s was that behavior of the fatigue life increase. In the former case the fatigue life continuously increased, whereas in the latter case the fatigue life initially decreased then increased.

As a result of the potential benefit of running mean strains, two studies (Pelton et al., 2008; Tolomeo et al., 2000) incorporated Finite-Element Analysis (FEA) into fatigue analysis. Each group (Pelton et al., 2008; Tolomeo et al., 2000) performed fatigue tests on NiTi components to gain an understanding of material behavior. Then NiTi components were designed like parts of an endovascular stent, and the deformation was simulated at various strains to determine the associated stress response at critical points in the component. The stress and strain values at the critical location of the stent were then used to calculate a constant-life diagram (Pelton et al., 2008; Tolomeo et al., 2000). These diagrams are made of two axes: a horizontal ε_a axis and a vertical ε_m axis. The data plotted is then the predicted combination of ε_a and ε_m that would reach a run-out criterion, e.g. 10^7 cycles. Both data sets have been plotted in one diagram in Figure 7. from (Mahtabi et al., 2015a).

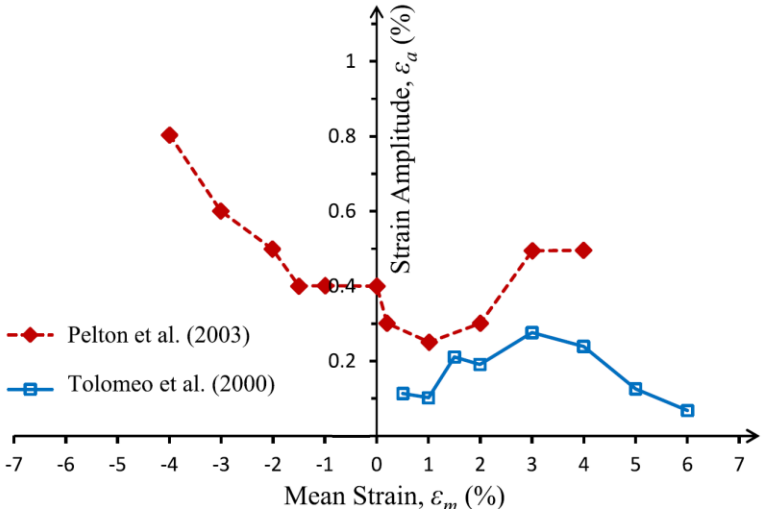

Figure 7 Constant life diagrams from (Pelton et al., 2003) and (Tolomeo et al., 2000) from (Mahtabi et al., 2015a)

Runciman and associates presented a modified coffin-manson type approach to modeling various loading types in NiTi alloys (Runciman et al., 2011). They define an equivalent transformation strain as the difference between the von Mises total strain and the von Mises elastic strain. The equivalent transformation strain amplitude is then modelled as proportional to the fatigue life, N_f raised to the negative one-half power (Runciman et al., 2011). The predictions from the model work reasonably well for torsional and bending data. However, the model does not correlate well to axail fatigue data (Mahtabi et al., 2015a).

Another model proposed in the literature was that of Moumni et al. They (Moumni et al., 2009) proposed an energy based damage parameter to capture the effects of the complex stress-strain response. The parameter developed in the study (Moumni et al., 2009) is the dissipated strain energy density, which is the area inside a hysteresis loop from one loading/unloading cycle. They found this parameter to work well for low-cycle

axial data, but did not report on high cycle or torsional fatigue data. Since high cycle fatigue primarily occurs in the austenitic linear elastic region of the stress-strain curve the model proposed may have issues. The hysteresis loop is virtually linear, i.e. no enclosed area, which would lead to no damage accumulation.

Mahtabi et al. (Mahtabi et al., 2015b) investigated the effects of mean strain of the fatigue behavior of superelastic NiTi by varying R_ε. The results from this study (Mahtabi et al., 2015b) seem to contradict the findings of previous studies (Morgan et al., 2004; Tabanli et al., 1999, 2001) by reporting a detrimental effect on the fatigue life. However, the results from this study (Mahtabi et al., 2015b) are in agreement with the previous findings. The difference arises from the use of R_ε to vary the mean strain. Due to the nature of the R_ε parameter, when it increases both ε_a and ε_m are increased simultaneously. Since both are increased the mechanical response is not directly analogous to the previous studies (Morgan et al., 2004; Tabanli et al., 1999, 2001). Other key findings from this study (Mahtabi et al., 2015b) include the inability of many common mean strain correction models to account for the stress plateau, the amount of strain hardening and mean stress relaxation with respect to ε_{max}, and the impact of residual martensite on the fatigue behavior.

Concluding Remarks

Superelastic NiTi is an extremely complex material system. Due to the intricate nature of the stress plateau in the mechanical response and the direct, influential relationship of the microstructure to mechanical response of superelastic NiTi is challenging to account for in design. Any attempt to study the fatigue behavior of superelastic NiTi should be approached methodically and precisely. Data analysis must

also be well researched and thorough, as understanding the underlying mechanisms and the general physics of the situation are necessary to provide reasonable modeling of fatigue behavior.

CHAPTER III

EXPERIMENTAL SETUP

Material

Medical grade NiTi, which has a 50.8% Ni and 49.2% Ti in atomic percent. The specimens were machined from 10 mm NiTi rods into dogbone specimens with a gauge diameter of 7 mm, as shown in Figure 8. Heat treatment was applied after the specimens were machined. The samples were aged by immersion in a salt bath at 550˚C for 2 minutes followed by quenching in ice water. The quenching step was included to ensure the NiTi specimens had an A_f temperature below room temperature and to create precipitates that stabilized the superelastic behavior (Gall et al., 1999a). The other parameters of the heat treatment were determined using a trial and error method starting with recommendations from Pelton et al.'s study (Pelton et al., 2000). The end result was specimens that exhibited stable, reproducible stress-strain behavior. The samples were then mechanically polished to a surface finish with an average roughness factor R_a = 0.693 μm. This was done in order to reduce the effects of surface finish on the fatigue resistance of the specimens.

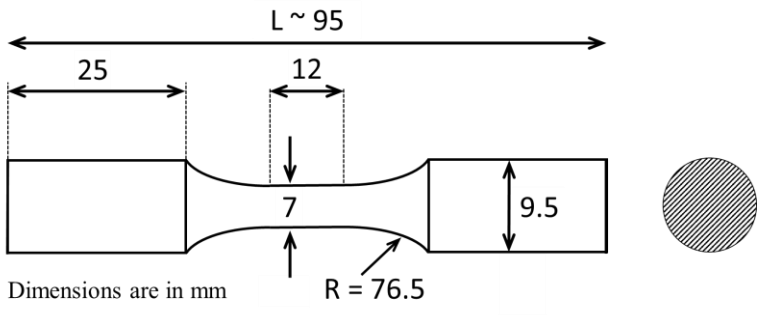

Figure 8 Diagram of specimen used in cyclic tests

Fatigue Testing Parameters

An MTS 810 servo-hydraulic uniaxial fatigue machine was employed to cyclically load the specimen using a strain-control from data taken by an extensometer. The testing was conducted at room temperature, ~24˚C. The frequency of each test was determined such that the strain rates would be consistent at about 0.036 mm/mm/s. Testing occurred at two different strain amplitude, ε_a, levels of 0.4% and 0.2%. Various ε_m tests were run at each ε_a level in order to see the effect of ε_a on the fatigue behavior in conjunction with ε_m. For ε_a = 0.4% the ε_m values tested were 0.4%, 0.8%, 2.2%, and 3.8%. For ε_a = 0.2% the values of ε_m were 0.27%, 0.53%, 1.47%, 2.53%, and 3.8%. A summary of the testing information can be found in Table 1.

Table 1 Testing information summary

Strain Amplitudes, ε_a (%)	Mean Strain levels, ε_m (%)				
0.20	0.27	0.53	1.47	2.53	3.80
0.40		0.40	0.80	2.20	3.80

The ε_m were chosen so that specimens would experience different volume fractions of martensite. For a breakdown of ε_m values and the regimes of the stress-strain curve where they lie see Table 2. These ε_m values were selected based on the mechanical response of the tension test of superelastic NiTi reported in (Mahtabi et al., 2015b). The monotonic tension test stress-strain plot from that study is shown in Table 2Figure 9. The values for various material properties found with this data are reported in Appendix A. The construction of the experiment was made to investigate the reported beneficial effect of tensile mean strains by doing two things (Morgan et al., 2004; Tabanli et al., 2001). First, the experiment is designed to identify the conditions for beneficial effects. Second, the experimental data is analyzed for both macro- and microscopic features that contribute to this behavior.

Table 2 Regimes of the mechanical response of Superelastic NiTi where ε_m values fall

Regime	Austenitic Linear Elastic	Beginning Stress Plateau	Mid Stress Plateau	End Stress Plateau
Mean Strain (%)	0.27, 0.40, 0.53, 0.80	1.47	2.20, 2.53	3.8

Microscopy Techniques

After a specimen had failed, the fracture surfaces were removed using a slow speed diamond saw. The cut was made about 1.5 to 2 mm from the fracture surface to avoid effects of local plasticity. After the fracture surfaces were mounted and sputter

coated, a sectioning cut was made. This cut removed a sample of the specimens gauge section for microstructure analysis using various techniques. The sectioned pieces were then cold-mounted in epoxy and polished mechanically. The polishing was performed on a Struers TegraPol-11 polisher with a TegraForce-1 specimen mover. The first step used a 1200 grit SiC pad with water and an applied force of 20 N at a rotation speed of 300 rpm. This step was followed by using an MD Largo pad with 9 µm Allegro suspension under 20 N and a rotation speed of 150 rpm. The third step has the same parameters as the second with the exception of the pad and suspension. This step used an MD Dac pad with the 3 µm Dac suspension. The final step required an MD Chem pad and OPS solution under 15 N rotating at 150 rpm. Those steps were followed by about 4 hours of vibratory polishing.

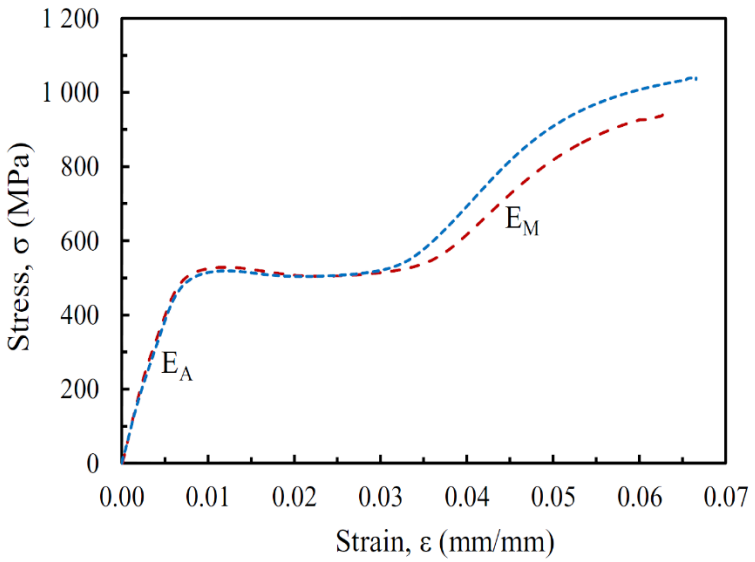

Figure 9 Stress-strain plot of monotonic tension test (Mahtabi et al., 2015b)

Fracture surfaces were studied using a scanning electron microscope (SEM). For microstructural results, optical microscopy was employed using a Leica DM ILM microscope for qualitative examination of phases present. For optical microscopy the samples were etched in a HF + HNO_3 +H_2O solution for approximately 10s. X-ray diffraction (XRD) was used to determine the behavior the bulk material microstructure as well as the lattice parameters for the austenitic phase of superelastic NiTi. The lattice parameter for austenite was used in electron backscatter diffraction (EBSD). The lattice parameters of the martensitic phase could not be determined solely from XRD for reasons that will be discussed in the next chapter.

EBSD was utilized to quantify the volume fraction of residual martensite, however this proved difficult without having the lattice parameters. Lattice parameters for martensitic NiTi were taken from the literature (Otsuka and Ren, 2005). The values reported were unable to capture the martensitic phase in the EBSD scans, which is most likely due to the severe lattice distortion around the residual martensite due to local plastic deformation, so an alternative method was found. Since EBSD only scans a portion of the sample's surface, multiple scans of each sample were taken at various locations to ensure the analysis of at least 700 grains in accordance with standard ASTM E112 (ASTM, 2004). The gray scale images from the scans were then analyzed in ImageJ (Schneider et al., 2012), an image processing software, to estimate the volume fraction of martensite.

CHAPTER IV

RESULTS AND DISCUSSION

Fatigue Results

The mean strain-life results from the fatigue tests are presented in Figure 10. For typical metallic material behavior, the plot would have a power series decay starting at the elongation to failure at the y-intercept and decreasing with increasing fatigue life. That behavior would demonstrate purely detrimental effects of mean strain. However the behavior of superelastic NiTi exhibits a beneficial effect of tensile mean strain near the end of the stress plateau, i.e. $\varepsilon_f^{AM} = 3.8\%$.

In this study, the beneficial effects become less noticeable with increasing ε_a. The fatigue life behavior for both amplitudes initially decreases with increasing ε_m until approximately $\varepsilon_m \sim 1.5\%$. Beyond that point the fatigue life performance improves or remains the same with increasing ε_m up to 3.8%. Also of note is the location of the relative minimum of the fatigue life in Figure 10 around $\varepsilon_m = 1.5\%$. From Table 2 it can be seen that this minimum corresponds to the onset of A → M phase transformation, and this occurs regardless of strain level. The behavior of the NiTi in this study behavior similar to that of Tabanli et al.'s data (Tabanli et al., 1999, 2001) despite differing sample types, differing treatment processes, differing testing conditions, and differing superelastic behavior, i.e. plateau stress value and range of plateau strain.

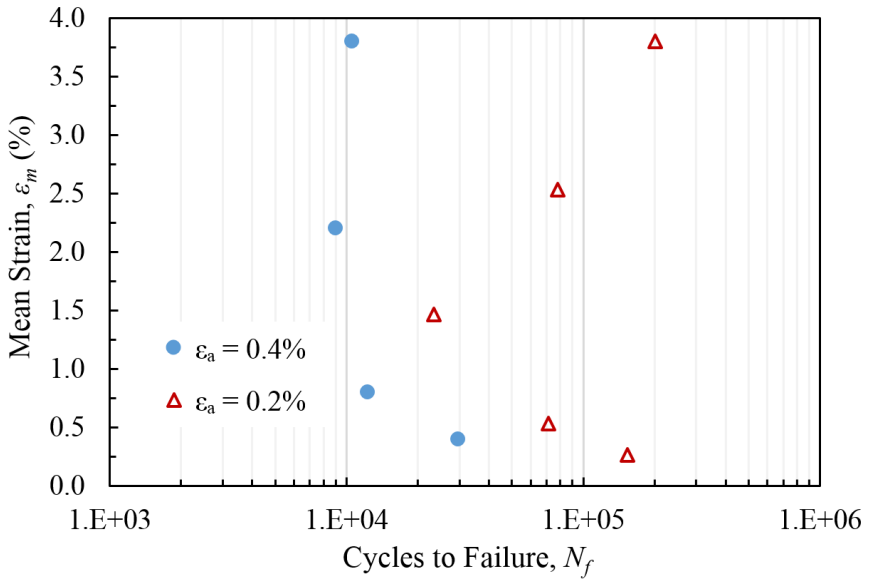

Figure 10 Mean strain-life plot indicating the longer fatigue lives for certain combinations of tensile mean strain and strain amplitude for larger mean strains

Fatigue Analysis

The results from the mean strain-life indicate that, in contrast to conventional metals, the fatigue life of superelastic NiTi does not necessarily decrease with increasing mean strain. When tested under large ε_m (i.e. $\varepsilon_m > 1\%$), cyclic loading with smaller ε_a NiTi experienced a longer fatigue life. The beneficial effects can be seen as a result of cyclic stress-strain response of superelastic NiTi. The beneficial effects were seen in specimens tested on the stress-plateau, and the effect was more pronounced for specimens tested at the end of the stress plateau, i.e. $\varepsilon_m = 3.8\%$.

The behavior of superelastic NiTi tested in this study can be understood by examining the cyclic deformation of specimens in hysteresis loops. Figure 11 is a plot of the hysteresis loops for all the ε_m test values conducted at $\varepsilon_a = 0.2\%$. Each of the five

different ε_m values are shown with three hysteresis loops. The first cycle's loop, the tenth cycle's loop, and the stable, i.e. mid-life, cycle's loop are shown to indicate the evolution of the stress-strain response. The ε_m value of each hysteresis loop is indicated above the data while the corresponding N_f is shown below. The effect of tensile mean strain and microstructure can be seen on the stress plateau. Starting with the ε_m = 1.47% (blue) data set, which is just past ε_s^{AM} = 1.0%, had the shortest fatigue life of all the ε_a = 0.2% tests. From there the tests cycled at increased ε_m increased in N_f. It is noteworthy that the tests conducted in this study were tested on the loading portion of the stress-strain curve with no pre-straining applied.

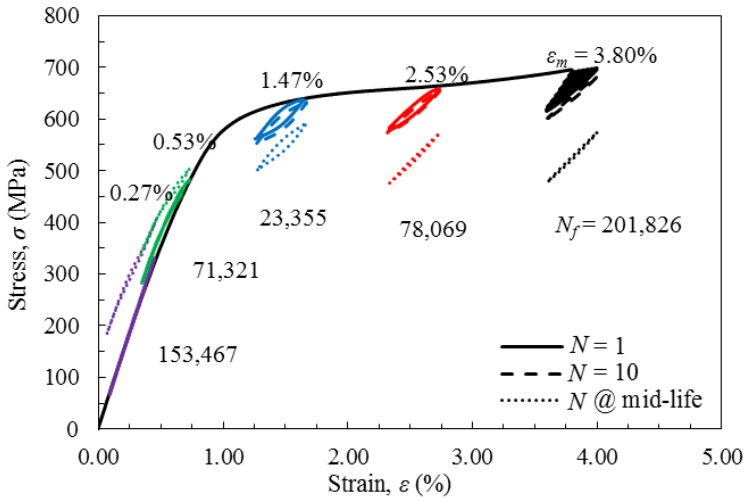

Figure 11 The hysteresis loops for ε_a = 0.2% and ε_m = 0.27% (purple), 0.53% (green), 1.47% (blue), 2.53% (green), and 3.80% (black) for the first cycle (solid line), tenth cycle (dashed line), and stable cycle (dotted)

With that in mind it is clearly seen in Figure 11 that the σ_a (the change in height of the hysteresis loop) for tests conducted on the stress plateau are significantly lower than

those in the austenitic linear elastic region. Table 3Figure 12 illustrates the differences in the stress amplitudes from the austenitic linear elastic region and the stress plateau. Both Table 3Figure 12 (a) and (b) have the same ε_a = 0.2%, but (a) has a ε_m = 0.53% while (b) has a ε_m = 3.8%. To facilitate the comparison, the stress axes of both Table 3Figure 12 (a) and (b) feature the same scale (same stress range, 550 – 300 = 250 and 650 – 400 = 250). As seen in the figure the specimen from the austenitic linear elastic region, i.e. Table 3Figure 12 (a), has a σ_a = 84 MPa compared to that of the specimen from the stress plateau, i.e. Table 3Figure 12 (b), which has a σ_a = 49 MPa. The σ_a experiences a 42% reduction when on the stress plateau.

This response is not unexpected since at the stress plateau there is little variation in the stress for a wide range of strains. To quantify: the stress plateau in this study begins at ε_s^{AM} = 1.0% and ends at ε_f^{AM} = 3.6% which gives a strain range of 2.6% strain. The stress range in this region between σ_s^{AM} = 500 MPa and σ_f^{AM} = 600 MPa is 100 MPa. On the other hand, for the linear austenitic region the change in stress is large for a smaller strain range. Starting at σ = 0 MPa and ε = 0% the stress increases 500 MPa to σ_s^{AM} while the strain only goes to ε_s^{AM} = 1.0%. The average σ_a response of each test is reported in Table 3. The average σ_a of a sample tested on the stress plateau, i.e. $\varepsilon_s^{AM} < \varepsilon_m < \varepsilon_f^{AM}$, is shown to be less than half of the average σ_a for a sample tested in the austenitic linear elastic region, i.e. $\varepsilon_m < \varepsilon_s^{AM}$. The indication of this data is that stress, specifically the cyclic component of stress, i.e. σ_a, is more influential on the fatigue resistance of superelastic NiTi than strain. This finding is in agreement with other studies (Mahtabi and Shamsaei, 2017; Mahtabi et al., 2015b; Moumni et al., 2005). Since the stress response, σ_a and σ_m, are nearly the same across samples tested on the stress plateau the

expectation would be for the fatigue lives to be similar. This expectation, however, does not match the observed data. It is more likely that stress effects only cause the detrimental aspect of tensile mean strains to be mitigated.

Table 3 Stress amplitude response data

Austenitic Linear Elastic Range			Phase Transformation Range		
ε_a (%)	ε_m (%)	σ_a (MPa)	ε_a (%)	ε_m (%)	σ_a (MPa)
0.2	0.27	112.52	0.2	1.47	45.50
0.2	0.53	83.94	0.2	2.53	48.45
			0.2	3.80	48.75
0.4	0.4	199.40	0.4	2.20	73.59
0.4	0.8	145.85	0.4	3.80	82.75
Average		135.43 ± 42.94	Average		59.80 ± 15.31

The difference testing on the loading plateau (solid blue line) versus testing on the unloading plateau (dashed red line) are highlighted in Figure 13. As mentioned previously, to conduct a test on the unloading plateau requires the specimen to be overstrained then allowed to unload until the desired testing parameters are reached. Two hypothetical responses for samples with identical testing parameters, e.g. ε_m and ε_a, are shown on the schematic. If the ε_a is small enough that the change in stress between the two stress plateaus is greater than the σ_a, then the stress response of each test will be different. Another aspect worth noting is the loading and unloading stress plateau values could forces upper and lower limits for σ_m for tests that fall between the A ↔ M threshold strains, i.e. ε_s^{AM} and ε_f^{AM}.

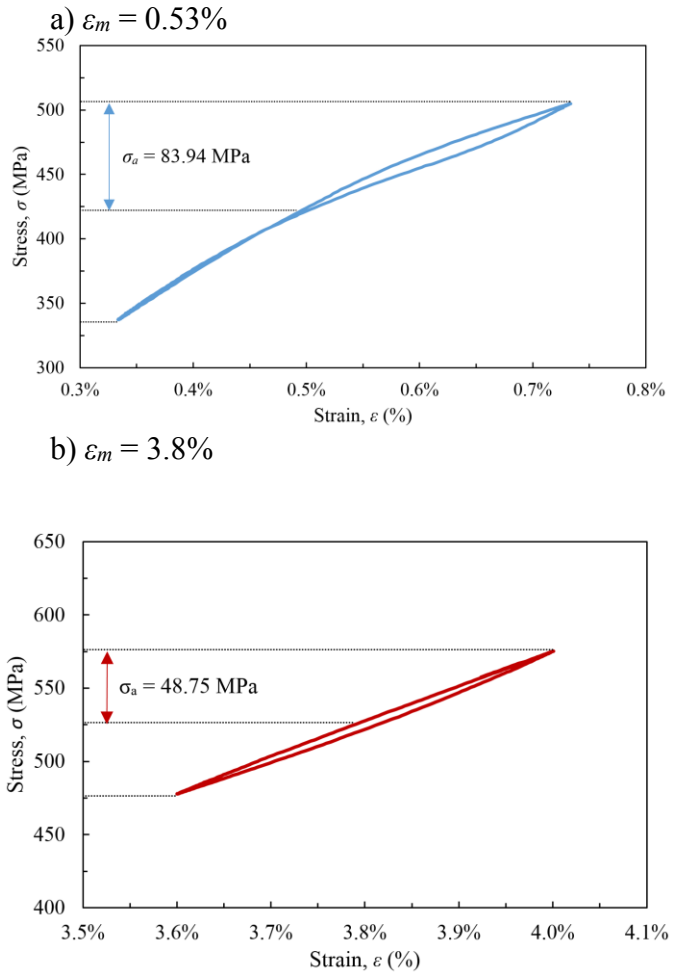

Figure 12 Stable cycle stress-strain response of the material tested at two different mean strain levels and ε_a = 0.2%, indicating the different sizes of the hysteresis loop and stress levels: (a) ε_m = 0.53% and (b) ε_m = 3.8%

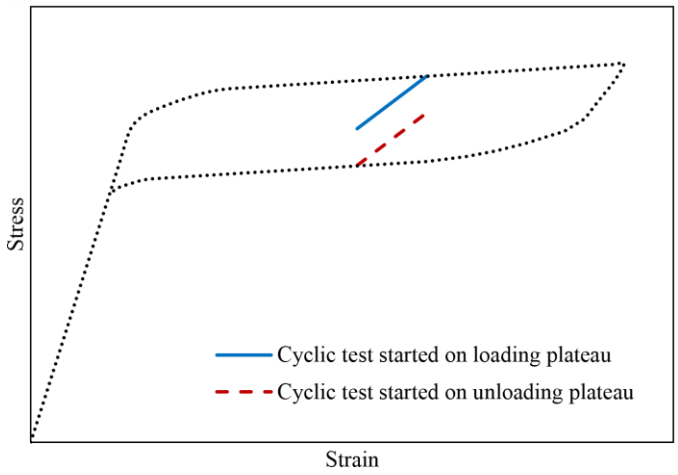

Figure 13 Schematic of cycling on the loading plateau versus the unloading plateau (i.e. after overstraining)

Another key feature of the stress response of samples tested on the stress plateau was mean stress relaxation. This phenomenon occurs under mean strain, ε_m, loading and is defined by a reduction in the mean stress, σ_m, over time as the specimen is cyclically loaded (Stephens et al., 2000). It is important to note that mean stress relaxation is different from cyclic softening and can therefore occur in the presence of cyclic hardening, which NiTi experiences. The mean stress relaxation can be seen in Figure 11 as the data sets for specimens on the stress plateau (blue, red and black) all shift down with respect to the stress axis. The stable cycle responses (dotted loops) of these tests are all significantly lower than the first and tenth cycle loops. This means that σ_m, and the overall stress state, have decreased with increasing cycles. To better illustrate mean stress relaxation Figure 14. Figure 14 plots the normalized mean stress versus number of cycles by taking the mean stress recorded at any given cycle, σ_{mN}, and normalizing, i.e. dividing, it by the σ_m of the first cycle, i.e. N=1 which gives σ_{m1}. The mean stress

relaxation data shows that the relaxation saturates for samples after about 1000 cycles. In Figure 14 it can be readily observed that the mean stress relaxes more for ε_m = 2.53 and 3.8% when compared to ε_m = 1.47%. The test conducted with ε_m = 1.47% only experienced a 13% reduction in mean stress at saturation compared to the about 20% reduction at saturation for the other two tests.

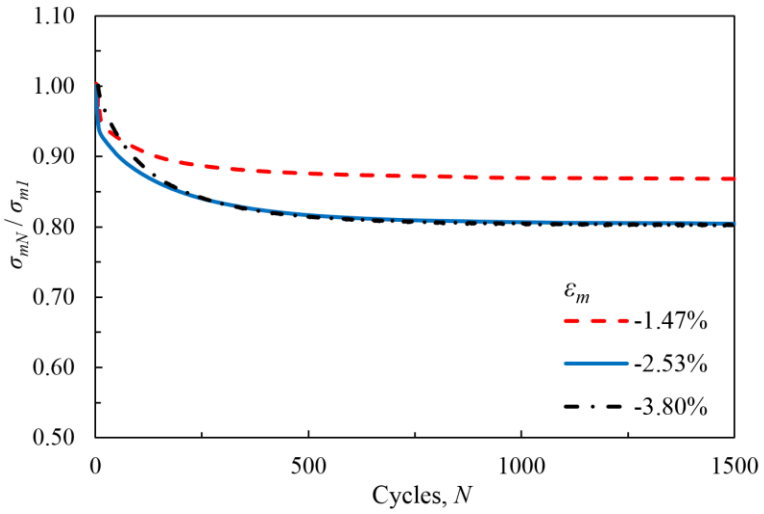

Figure 14 Evolution of the mean stress level at different mean strain levels

The significance of the stress relaxation is twofold. One is that the σ_m does not fully relax, i.e. σ_m = 0, and therefore is a contributing factor to the fatigue behavior of superelastic NiTi. Since σ_m contributes to the fatigue behavior it must be accounted for when attempting predictive modeling (Mahtabi and Shamsaei, 2017). The second implication of the relaxation data is that the specimens tested with higher ε_m, which have higher volume fractions of martensite, experienced more relaxation. This means that the more martensitic a sample is the more stress relaxation it may experience, up to a point.

The difference between the samples loaded at ε_m = 2.53 and 3.8% is negligible and suggests a limit to mean stress relaxation even for very large strains.

The mean stress relaxation data for specimens tested on the stress plateau, i.e. $\varepsilon_s^{AM} < \varepsilon_m < \varepsilon_f^{AM}$, across both ε_a parameters are listed in Table 4. Table 4 also includes some data tested with ε_a = 0.3%. In terms of raw numbers the tests with the highest ε_m, i.e. 3.8%, tend to experience the largest overall amount of mean stress relaxation. In terms of normalized numbers, i.e. percentages, these tests, ε_m = 3.8%, also had the largest percent of mid-life σ_m relaxation (decrease in σ_m divided by σ_m of the mid-life cycle). Additionally, they possessed the fastest rates of relaxation to stable cyclic response with respect to number of cycles. Therefore, one might conclude that the relative amount of mean stress relaxation is dependent on the amount of martensite in the material. The martensitic volume fraction can be approximated from the stress-strain parameters involving A → M phase transformation, i.e. ε_s^{AM}, ε_f^{AM}, σ_s^{AM}, and σ_s^{AM}. In a previous study (Brinson et al., 2004) determined the approximate volume fraction of martensite to be 65 – 70% at the end of the phase transformation plateau. They observed this using an in situ, polarlized optical microscopy. Assuming volume fraction of martensite is assumed to be 0% before the onset of phase transformation and the rate of transformation along the stress plateau is linear the martensitic content could be approximated. This would only require knowledge of 3 parameters: ε_s^{AM}, ε, and ε_f^{AM}, where ε is the applied strain. A diagram of how this could work is presented in Table 4Figure 15.

Table 4 Analysis of mean stress relaxation data for different test conditions

ε_a (%)	ε_m (%)	Relaxation to Stable Response (MPa)	Relaxation Rate (MPa/cycle)	Relaxation at Failure
0.2	1.47	58.54	0.05	58.5
0.2	2.53	96.35	0.08	96.4
0.2	3.80	123.94	0.11	134.0
0.4	2.20	42.93	0.04	42.9
0.4	3.80	99.78	0.10	102.3

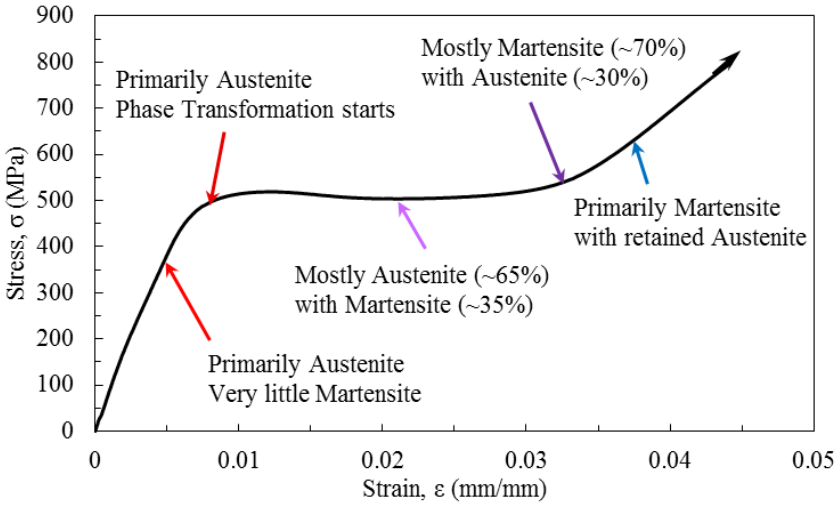

Figure 15 Diagram of stress-strain curve with volume fractions approximations of microstructure

To demonstrate the difficulty with analyzing superelastic NiTi fatigue data, Figure 16 represents the σ_a versus N_f with a semi-log scale. The data shown in Figure 16 has no concrete trend in the stress-life data. The lack of a consistent trend in Figure 16 arises from the variation in N_f of the specimens despite having similar σ_a, σ_m, and ε_a, but different ε_m. The σ_a of specimens tested on the plateau is partially responsible for this trend. Figure 11 shows that, despite the differences in mean strain, the tests conducted on

the stress plateau have similar σ_a and σ_m. Other studies (Melton and Mercier, 1979b; Moumni et al., 2005) have noted a fairly linear relationship of σ_a and N_f in similar plots. The difference in the data from this study to that of other studies (Melton and Mercier, 1979b; Moumni et al., 2005) is that this data was not generated by varying R_ε / R_σ, R_ε = ε_{min} / ε_{max} and R_σ = σ_{min} / σ_{max}. Also, specimens on the stress plateau, e.g. ε_m = 1.47, 2.53, and 3.8%, had similar σ_a, σ_m, and R_σ, i.e. σ_m ~ 530 MPa, σ_a ~ 47.5 MPa, and R_σ ~ 0.83, with vastly different fatigue lives, N_f = 23,355; 78,069; and 201,826 cycles, respectively.

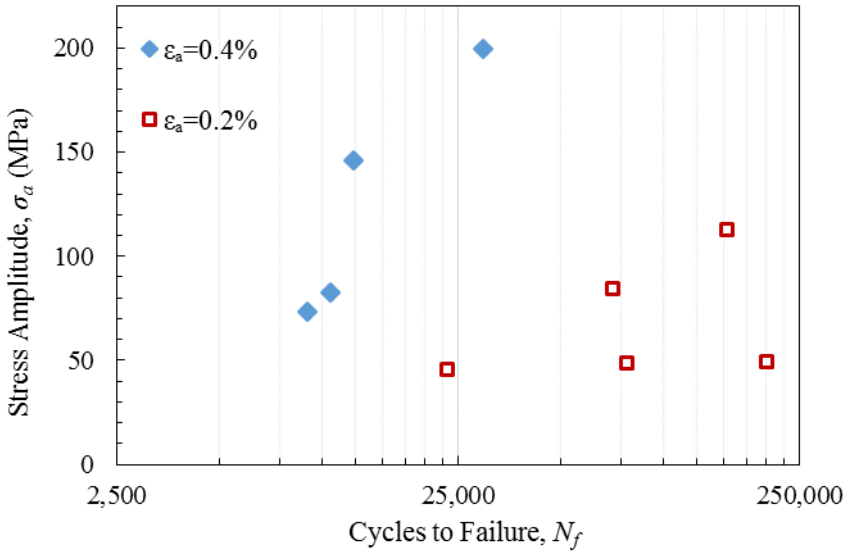

Figure 16 Stress amplitude-life plot showing no trend in fatigue behavior based on the stress amplitude

The significance of mean stress relaxation to the fatigue behavior of superelastic NiTi is that tests with greater ε_m, e.g. ε_m = 3.8%, can reach a stress response similar to those near the start of the stress plateau, e.g. ε_m = 1.47%. In this study the stable responses with σ_a within ~ ±3.5 MPa and σ_m within ~ ±20MPa. These similar stress

responses would suggest at least similar fatigue lives, but that will be discussed more in a later section. One final noteworthy observation from Table 4 shows the mean stress relaxation in terms of percentage appears to be independent of ε_a, as seen in the data for the ε_m = 3.8% data. The average relaxation percentage of ε_m = 3.8% was 17.42% ± 1.39% reduction in σ_m. Going back to a previous statement, the specimens tested on the stress plateau had nearly identical stress responses, σ_a within ~ 3.5 MPa and σ_m within ~ 20MPa. However, ε_a = 0.2% tests the variation in N_f was almost an order of magnitude from the onset of phase transformation, i.e. ε_m = 1.47%, to the end of the stress plateau, i.e. ε_m = 3.8%. This result suggests that there is another mechanism involved in driving the beneficial effect of tensile mean strains in NiTi.

Microstructure Observation Results

Examination of the sectioned and etched specimens' cross-sections revealed the presence of residual martensite in all the specimens. This included the samples that were tested in the austenitic linear elastic region, which theoretically should not have experienced phase transformation. Images from a specimen tested in the austenitic linear elastic region (i.e. $\varepsilon_{max} < \varepsilon_s^{AM}$) and on the stress plateau (i.e. $\varepsilon_{max} > \varepsilon_s^{AM}$) is shown in Figure 17 (a) and (b), respectively. The martensitic phase appears as the dark lathe structure within the grains in these figures. Precipitates are seen as the small dark dots in the austenitic grains. Since optical microscopy does not allow for robust quantification of the microstructural volume fractions in the sample, other analytical techniques were employed.

(a)

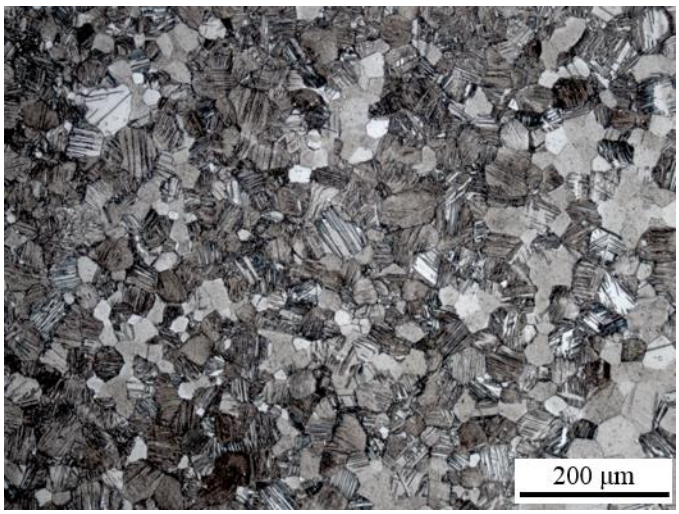

(b)

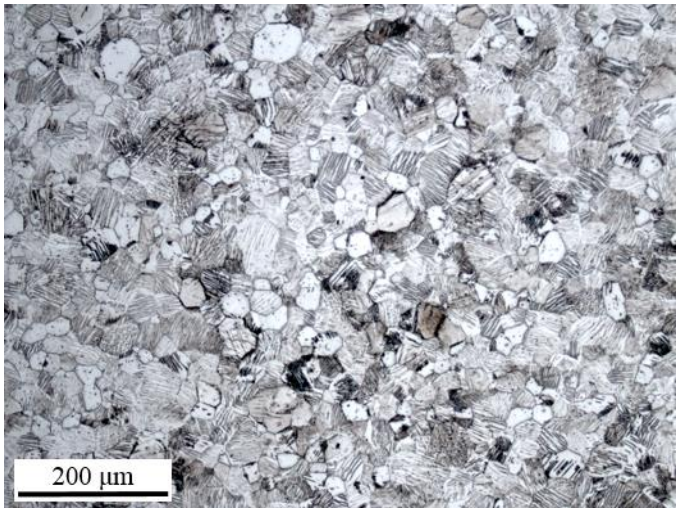

Figure 17 Optical microscopy images of the two specimens showing the residual martensitic phase in the loaded material: (a) ε_a = 0.4% and ε_m = 0.4%. and (b) ε_a = 0.2% and ε_m = 1.47%

X-ray diffraction (XRD) was then used to characterize the crystal structure of superelastic NiTi by quantifying the lattice parameter of the austenitic phase. The martensitic phase of NiTi proved impossible to determine the lattice parameters due to

the low symmetry of a monoclinic unit cell, which martensite is known to be (Otsuka and Ren, 2005). A monoclinic crystal needs four independent lattice parameters to fully define. To accomplish this there must be four independent equations relating to a measurable quantity to fully define a martensitic NiTi crystal. However, XRD only determines one independent, measurable value, namely the Bragg angle. The Bragg angle can be related to the inter-atomic spacing (d-spacing) through Bragg's Law. The results from an XRD scan are provided in Figure 18. From these results the Bragg angles can be found by looking at the angle that corresponds to the peaks in the intensity. From here the Bragg angles can be related to the lattice parameter of a cubic lattice, i.e. NiTi (Otsuka and Ren, 2005). This is accomplished by incorporating Bragg's law, given by:

$$2d\sin(\theta) = n\lambda \quad (1)$$

where d is the d-spacing of a given orientation of the crystal, θ is the Bragg angle, n is a positive integer, and λ is the wavelength of the radiation use in diffraction. In addition to Bragg's law the d-spacing relationship to the lattice parameter, given by the following for a cubic lattice:

$$d = \frac{a}{\sqrt{h^2+k^2+l^2}} \quad (2)$$

where d is the same as before, a is the lattice parameter of a cubic structure, and h,k, and l are Miller indices denoting orientation (Smith and Hashemi, 2006). By substituting equation 1 into equation 2 the lattice parameter can be found from the XRD data. The results of these calculations can be found in Table 5. The calculated lattice parameter, *a* = 3.012 Å, is consistent with the literature (McKelvey and Ritchie, 2001; Otsuka and Ren, 2005) and the ICDD crystal database (Reyes-Mena et al., 2005). The lattice parameter was subsequently used as an input parameter for the EBSD analysis.

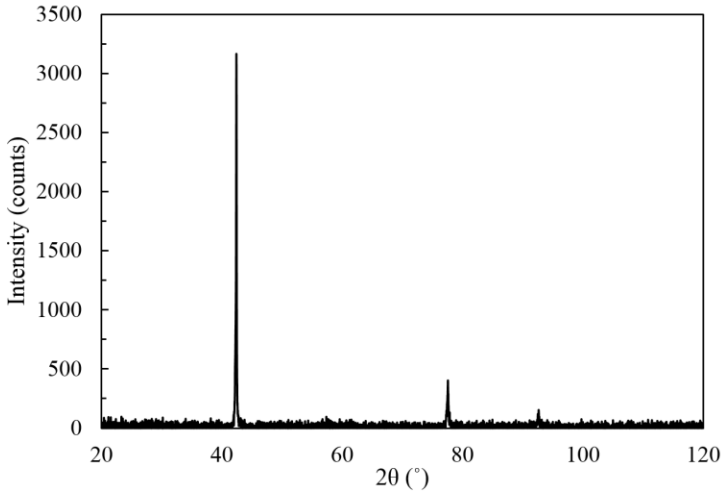

Figure 18 XRD scan of specimen tested at ε_m = 3.80% and ε_a = 0.2%

Table 5 XRD results for austenitic NiTi used in this study

2θ(°)	(h k l)	d-spacing (Å)	*a* (Å)
42.40	(1 1 0)	2.13	3.012
77.58	(2 1 1)	1.23	3.012
92.68	(2 2 0)	1.065	3.012

The martensitic phase had no discernable peaks in the scans, and has four unknown lattice parameters. Without the d-spacing and peaks the martensitic lattice parameters could not be found. Even if there were peaks seen, a monoclinic cell has four unknowns to only one known Bragg angle. This means that even with peaks from martensite a numerical solver would be needed to find viable solutions that would need to be compared to other microstructure data on B19' NiTi. Therefore the martensitic lattice parameters were not calculated in this work.

Using the lattice parameter found by XRD, electron backscatter diffraction (EBSD) was utilized to study the grain size and of the austenitic phase. EBSD served

two primary purposes to this study. The first was verifying the lattice parameter found by XRD to give confidence in the results of the diffraction data from XRD and EBSD. The second was to provide a means of quantifying the volume fraction of residual martensite in the samples. Since martensitic lattice parameters were not determined, values from (Otsuka and Ren, 2005) were used, however they did not provide viable results. For that reason the volume fraction analysis was performed by implanting an image processing software, ImageJ, to quantify the volume fraction of martensite digitally. Grayscale images from the EBSD scans, like the one shown in Figure 19, were used in this process.

The results from the digital processing for ε_a = 0.2% data are given by Table 6. The data set for ε_a = 0.2% was chosen for study since it demonstrated the largest range in fatigue lives on the phase transformation plateau. If the fatigue life was related to the martensitic content, it is expected to be most evident for these samples. The data shows that the amount of residual martensite in the samples after fatigue failure to be relatively small (~ 8%) compared to expectations from the stress-strain behavior of the tests. The data also appears to be largely independent of mean strain since the ε_m = 3.8% sample had a similar volume fraction of martensite to the ε_m = 0.53% sample, 8.59% and 8.98%, respectively. As seen in the optical investigation, the EBSD data also revealed residual martensite in the samples tested below the ε_s^{AM}. This is likely due to stress concentrations in the material matrix. The causes of the stress concentrations include precipitates, which create favorable martensite formation to deformation (Gall et al., 1999a), as well as other inhomogeneities. Only one test (ε_a = 0.2%, ε_m = 1.47%) had more than 10% residual martensite when analyzed. This test was conducted in the early onset of A → M phase transformation on the stress plateau.

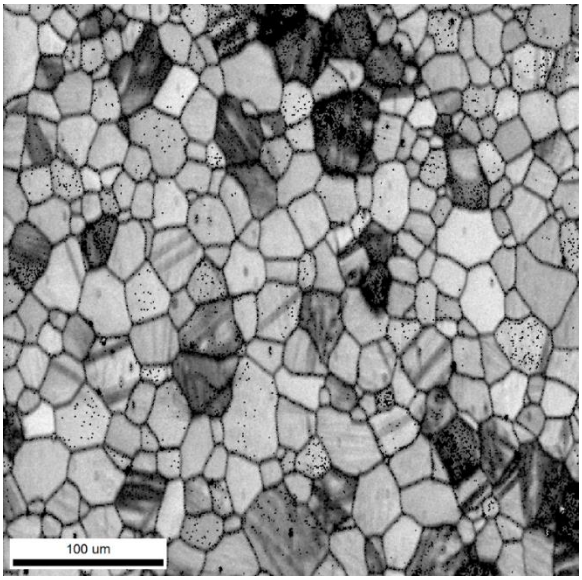

Figure 19 Grayscale image of EBSD scan for specimen tested at ε_m = 1.47% and ε_a = 0.2%

Table 6 Volume fraction of martensite phase based on EBSD scans

Test Paramters		Martensite (B19') volume fraction (%)					Fatigue Life
ε_a (%)	ε_m (%)	Scan 1	Scan 2	Scan 3	Scan 4	Average	N_f (Cycles)
0.2	0.27	7.28	8.58	3.33	5.07	6.07	151,467
0.2	0.53	2.20	10.75	12.46	10.50	8.98	71,321
0.2	1.47	23.53	15.24	6.29	16.31	15.34	23,355
0.2	2.53	6.72	8.50	8.08	10.94	8.56	78,069
0.2	3.8	6.27	9.77	8.94	9.39	8.59	201,826

Microstructure Analysis

As discussed earlier, the volume fraction of martensite appears to be a cause of mean stress relaxation in superelastic NiTi. Also mentioned previously is the stress-strain relationship to the volume fraction of martensite present in the material. It has been reported (Brinson et al., 2004) that the volume fraction of martensite in superelastic NiTi near the end of the stress plateau, i.e. ε_f^{AM}, is typically on the order of 60-70%. In

this study, the largest ε_m, 3.8%, would lie in this region and the strain on this specimen would oscillate between 3.4% to 4.2% or 3.6% to 4.0% for ε_a = 0.4% and 0.2% respectively. The specimens tested at that ε_m have had an average martensitic volume fraction comparable to 60-70% according to the study (Brinson et al., 2004). The amount of martensite present in the specimens has important implications about the fatigue behavior that will now be discussed.

The pronounced effect of tensile mean strains on the fatigue behavior for samples tested with smaller ε_a is contributed to by martensitic volume fractions. Referring back to Figure 10, the variation fatigue life with increasing mean strain is clearly seen in the ε_a = 0.2% data set. For the ε_a = 0.4% it is more difficult to tell. Comparing the fatigue lives of samples on the plateau for both ε_a = 0.4% and 0.2% make this effect of ε_a clear. Notably, the smaller strain amplitudes show greater sensitivity to tensile mean strain effects. For the ε_a = 0.4% data set ε_m = 3.8% (N_f = 10,603 cycles) was only slightly higher than that of ε_m = 2.2% (N_f = 9,051 cycles). That relates to a 17% improvement in fatigue performance, but would not imply beneficial effects alone. At most, it indicates a lack of sensitivity to ε_m. However, coupled with ε_a = 0.2% data it correlates to beneficial effects. That for the ε_a = 0.2% data set the ε_m = 3.8% (N_f = 201,826 cycles) is more than double that of ε_m = 2.53% (N_f = 78,069). Even over a smaller increase in strain the fatigue live improved much more drastically than the ε_a = 0.4% data. Extended to the start of the plateau where ε_m = 1.47% (N_f = 23,355 cycles) for ε_a = 0.2% and the improvement to ε_m = 3.8% is almost an order of magnitude. So now we relate that to microstructure.

Larger ε_m values result in larger volume fractions of martensitic NiTi in the material. Simultaneously the ε_a is oscillating, which has been shown to drive phase transformation fronts through the material (Iadicola and Shaw, 2002). For larger ε_a values, more material will be undergoing phase transformation in a cycle than for lower strain amplitudes. The movement of phase transformation fronts has been linked with minimal plasticity occurring in the material (Gall et al., 2002; Iadicola and Shaw, 2002; Norfleet et al., 2009). The plasticity is localized to the transformation front and its movement (Norfleet et al., 2009), which is related to ε_a more so than ε_m. Also, for a given ε_m, a larger ε_a would have more austenitic microstructure at the end of unloading than a smaller ε_a. This higher content of austenite may allow for more crack nucleation sites in superelastic NiTi since it has the worst fracture threshold properties of all NiTi phases (McKelvey and Ritchie, 2001). A recent study (Gloanec et al., 2010) has also linked crack initiation to interfaces between austenite and martensite due to dislocation accumulation, i.e. plasticity. This could explain the reason larger ε_a's experience a diminished beneficial effect, or experience a detrimental effect (Mahtabi et al., 2015b).

The values for residual martensite shown earlier in Table 6 were expected to follow the same trend as the ε_m. Namely, that specimens tested with higher ε_m would have more residual martensite in the volume fraction of each phase. A monotonic stress-strain curve generated by McKelvey and Ritchie (McKelvey and Ritchie, 2001) shows the complete degeneration of the superelastic property in NiTi when loaded past the yield point. The yield point refers to the point in the stress-strain curve past the martensitic linear elastic region. In their study (McKelvey and Ritchie, 2001) describe the situation where plasticity from dislocation accumulation causes internal stresses on NiTi grains.

These stresses cause enough distortional strain energy that the thermal energy is no longer capable of driving reverse transformation to austenite. However, in this study the applied strains are well below the yield, which means significantly less dislocation motion would be seen. Furthermore, the residual martensite in the presence of minimal plasticity may be subjected to a phenomenon referred to as "strain recovery" (Paradis et al., 2008). The phenomenon of strain recovery observed by Paradis et al. (Paradis et al., 2008) reportedly affects NiTi in a climate with an ambient temperature above A_f. The effect was that the residual strain, correlated to the residual martensite, was recovered in samples left above A_f over time. In this study samples were stored at room temperature, i.e. above A_f, after fracture and were therefore subject to the same thermal effect. The amount of time it takes for strain recovery to occur was reported to be as little as 5 seconds (Paradis et al., 2008). As a result the EBSD scans revealed residual martensite quantities did not correspond to the volume fraction of martensite that the specimens would have undergone during loading.

Fractography

Fracture surface analysis was carried out using a scanning electron microscope (SEM). Like other NiTi studies (Gall et al., 2001; James et al., 2005; Mahtabi et al., 2015b) the surfaces featured crack initiation near an inclusion close to the surface with a relatively small crack growth region. The fractured specimens typically exhibited a relatively smooth morphology, and became progressively rougher with increasing ε_m and ε_a. Additionally the area of crack growth was larger for specimens with lower ε_m and ε_a, which is typical in metal fatigue (Stephens et al., 2000). Figure 20 shows the crack growth region for multiple tests at various ε_a and ε_m. The largest crack growth region was

seen on the surface of the specimen loaded at ε_a = 0.2% and ε_m = 0.53% and was approximately 12% of the fracture surface's area. Contrastively the smallest region was about 2.4% of the surface area on the sample strained at ε_a = 0.4% and ε_m = 3.8%. All the other specimens fell within these bounds and generally followed the trend.

Another general trend in fatigue is that the fatigue life is longer when the fracture surface has a larger area of crack growth (Stephens et al., 2000). In the case of fatigue lives to crack growth areas, superelastic NiTi does not obey this rule of thumb. Superelastic NiTi's unique fatigue behavior in the presence of tensile mean strains, i.e. fatigue life improvement with increasing ε_m, is the source of this discrepancy. Since the fatigue life does not monotonously decrease with increases in ε_m, and higher ε_m, and ε_a, result in smaller crack growth regions the expectation should be that the trend does not hold. However, this poses a question to explain what is happening. If the crack growth stage is not lasting longer and therefore increasing the life, what is the cause of the longer fatigue life?

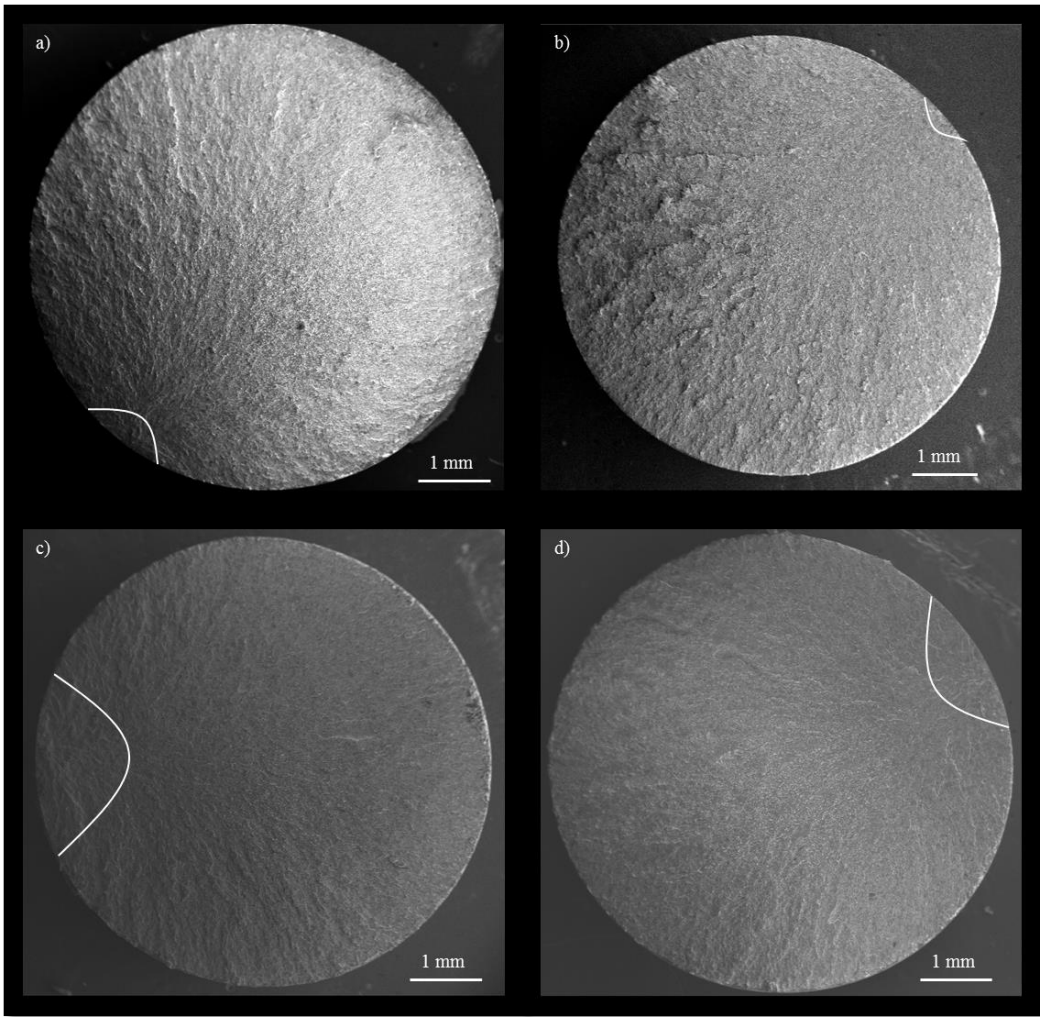

Figure 20 Fracture surfaces showing the crack growth regions inside the arcs shown for a) $\varepsilon_a = 0.2\%$ and $\varepsilon_m = 3.8\%$, b) $\varepsilon_a = 0.4\%$ and $\varepsilon_m = 3.8\%$, c) $\varepsilon_a = 0.2\%$ and $\varepsilon_m = 0.53\%$, and d) $\varepsilon_a = 0.4\%$ and $\varepsilon_m = 0.8\%$

There are two possible answers to the above question. One is that the material experiences less crack propagation per cycle once a crack has nucleated, or crack nucleation requires more cycles to occur. Since NiTi has been shown to follow the Paris law of crack growth (McKelvey and Ritchie, 2001; Stephens et al., 2000) and that different phases of NiTi have similar crack growth rates (McKelvey and Ritchie, 2001),

the first option is ruled out. Additionally, as stated in the previous section, McKelvey and Ritchie (McKelvey and Ritchie, 2001) reported that superelastic autenite has the worst fracture threshold properties of all the studied phases of NiTi. By contrast martensite, specifically thermal martensite, was reported to have the best fracture threshold properties, approximately 1.5 – 2.5 times greater than superelastic austenite (McKelvey and Ritchie, 2001). Therefore, the higher the martensitic content in a sample, the longer it can go before a crack initiates. It is also worth noting, that thermal martensite, i.e. martensite induced by lowering the temperature below M_f, may behave differently than stress-induced. Stress induced martensite generally forms so that the variants, i.e. orientations, are most suited to accommodate the applied load. Thermal martensite is more likely to form random variants scattered throughout the sample, thus stress-induced martensite may have slightly better fracture threshold properties. That said, higher martensite volume fractions are associated with larger ε_m, which corresponds well to the fracture surface and fatigue life data.

As mentioned before, cracks initiated near defects close to the specimen surface, however the defect size was not as influential as other parameters, e.g. ε_a and ε_m. The average defect size was found to be 28.08 ± 17.69 μm and ranged from 9.93 to 60.28 μm. The defect in the ε_m = 3.8%, ε_a = 0.4% was ~ 4 times larger than any other defect in ε_a = 0.4% data set, which may account for part of the less pronounced effect of tensile mean strains on larger ε_a's.

Micro-cracks were also observed around the initiation sites similar to another study (Mahtabi et al., 2015b). The density of these microcracks, i.e. the number of micro-cracks within 50 μm of the initiation site, tended to increase with increasing ε_m and

ε_a. Figure 21 shows a representative image of the initiation site with arrows denoting micro-cracks inside the 50 μm ring. The range of the microcracks in the vicinity of the inclusion went from 7 observed in ε_a = 0.2% and ε_m = 0.53% to more than 20 for ε_m = 3.8% across all data sets. This finding appears to contradict the claim that martensite has superior crack threshold properties since there are more micro-cracks. However, the observation of increased micro-crack density actually lends itself to the superior threshold properties of martensite.

Micro-cracks, i.e. cracks on the order of length of a grain diameter or shorter, do not behave in the same way as structurally large cracks (Chan, 2010). The stresses experienced by the ε_m = 3.8% tests were of a high enough magnitude to initiate micro-cracks. However, due to the superior properties of martensite with respect the fracture threshold, the microstructure was able to arrest crack growth before the micro-crack could grow to a structurally large crack. Samples with Austenitic microstructure were tested with similar or lower stress states, σ_a and σ_m, were less resistant to micro-crack growth. The micro-cracks did not experience arrested growth and propagated quickly to structurally large cracks. These large-cracks then grew to a critically unstable length and led to failure. This results in fewer micro-cracks in austenitic samples. For samples with the lowest mean strains, i.e. ε_m = 0.4 and 0.53%, had lower stresses and that results in fewer overall micro-cracks. Consider the ε_m = 3.8%, ε_a = 0.2% test, which had more than 20 micro-cracks compared to the 7 or so of the ε_m = 1.47%, ε_a = 0.2% test. The ε_m = 3.8% lasted ~175,000 cycles longer and had similar stresses, σ_a and σ_m.

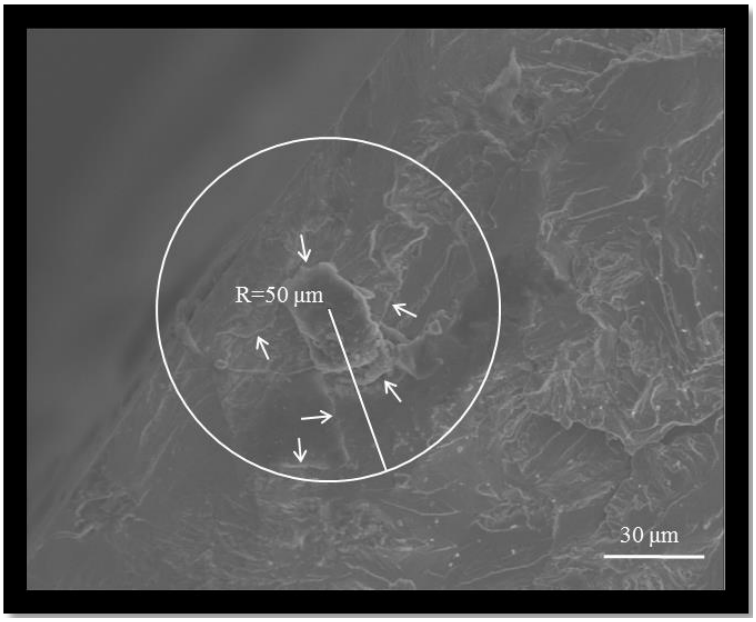

Figure 21 SEM image showing the region with 50 µm of the initiation site where the micro-crack density is measured. The specimen shown was loaded at ε_a = 0.2% and ε_m = 0.53%

Modelling

The complicated stress-strain behavior of superelastic NiTi, whether cyclic or monotonic, has made modeling the fatigue behavior difficult (Mahtabi et al., 2015b). Development of a robust prediction model for the fatigue behavior is a paramount consideration of fatigue analysis. Most classical fatigue models, e.g. Goodman, Morrow, Coffin-Manson, etc. use only one component, a stress or strain parameter, to model fatigue. It has been recently demonstrated in a study (Mahtabi and Shamsaei, 2016) that using only one parameter, stress or strain, is insufficient for NiTi fatigue modelling for reasonable life prediction. As a result, several studies in the literature developed and proposed energy models that consider effects of both stress and strain simultaneously (Kang et al., 2012; Mahtabi and Shamsaei, 2016; Moumni et al., 2005).

Of the energy models proposed by Moumni et al. (Moumni et al., 2005) and Mahtabi and Shamsaei (Mahtabi and Shamsaei, 2016) there is one primary difference. The model proposed by Moumni and co-workers includes only a dissipated energy parameter. Conversely, Mahtabi and Shamsaei's model has a dissipated energy term as well as another parameter for tensile elastic energy density. The tensile elastic energy density term in Mahtabi and Shamsaei's (Mahtabi and Shamsaei, 2016) work accounts for the effects of tensile mean stress and also enables robust fatigue life prediction in the austenitic linear elastic region. If dissipated energy, i.e. the area enclosed in a hysteresis loop, is the only damage parameter considered then linear elastic tests are predicted to never fail. The area enclosed in the hysteresis loop would be virtually zero. While necessary to account for mean strain effects, the dissipated energy parameter alone is not sufficient to modelling NiTi components under all loading conditions.

The model proposed by Mahtabi and Shamsaei (Mahtabi and Shamsaei, 2016) provided reasonably accurate predictions for NiTi components with comparable stress plateau values, i.e. σ_s^{AM}. More recently, they have extended the model to apply to NiTi alloys with a wide range of stress plateau values. This is necessary since NiTi alloys' material properties can vary widely due to high sensitivity of NiTi to processing and chemical composition. In a recent study (Mahtabi and Shamsaei, 2017) Mahtabi and Shamsaei proposed a cumulative strain energy density, ΣW_t, as a damage parameter given by:

$$\Sigma W_t = \sum_{i=1}^{N_f} (W_t)_i = \sum_{i=1}^{N_f} (W_d + W_e^+)_i \tag{3}$$

in which W_d is the dissipated strain energy density of each cycle, i.e. the area enclosed by the hysteresis loop. W_e^+ is the tensile elastic strain energy density of each cycle, and accounts for the effects of tensile mean stress on the fatigue behavior of superelastic NiTi. The value of W_e^+ for each cycle can be calculated using the following equation:

$$W_e^+ = \frac{\sigma_{max}^2}{2E_A} = \frac{(\sigma_a + \sigma_m)^2}{2E_A} \tag{4}$$

where E_A is the elastic modulus of superelastic NiTi in the austenitic linear elastic region.

This proposed damage parameter handles variation in cyclic deformation of superelastic NiTi and works for fatigue analysis. Therefore, this study has employed the model proposed by Mahtabi and Shamsaei (Mahtabi and Shamsaei, 2017) to analyze the beneficial effects of tensile mean strain on the fatigue resistance of superelastic NiTi. The results of these calculations are given by Figure 22. As can be seen in the Figure 22, the damage parameter accurately predicts the unique fatigue behavior of superelastic NiTi in the presence of tensile mean strains.

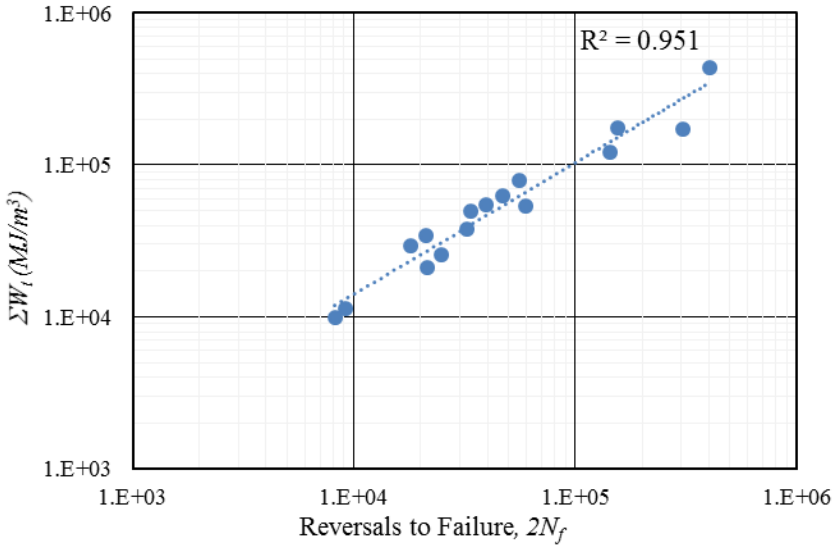

Figure 22 Cumulative total strain energy density, ΣW_t, versus fatigue life of specimens at different mean strains

CHAPTER V

SUMMARY AND CONCLUSIONS

Summary

NiTi, and other shape memory alloys, are growing in popularity in industrial applications due to superior material properties, namely superelasticity. Since many of these applications involve complex cyclic loads understanding the fatigue behavior of this material is paramount for robust, efficient design. Due to the eccentric nature of the stress-strain behavior of superelastic NiTi and the reversible thermos-mechanical phase transformation phenomenon the fatigue behavior of these alloys is incredibly complex (Mahtabi et al., 2015a; Robertson et al., 2012). When loaded under strains with a tensile mean strain component NiTi has been reported to experience an increase in fatigue life (Morgan et al., 2004; Tabanli et al., 1999, 2001), but not always (Mahtabi et al., 2015b). With that in mind this work investigate the effects of tensile mean strain on the fatigue behavior while looking to the microstructure for explanations into the physics of this phenomenon.

In this work it was observed that at low strain amplitudes the fatigue behavior of superelastic NiTi exhibited improvements under increased ε_m, for certain ranges of strain. This range of strain was related experienced the same σ_a and σ_m as some lower ε_m. Additionally the beneficial range of ε_m corresponded to higher volume fractions of martensitic NiTi, which both effects the cyclic stress-strain response as well as material

properties. Martensite and the phase transformation phenomenon both contribute to stress state that is comparable across the entire stress plateau through smaller σ_a and mean stress relaxation. Martensitic NiTi also possesses superior fracture threshold properties to superelastic austenite (McKelvey and Ritchie, 2001), which lengthens the crack nucleation stage of the fatigue life, thus providing a beneficial effect.

Conclusions

Based on observed data produced by the experiments in this work as well as an analytical probing of the microstructure the following conclusions have been drawn:

1. Mean stress relaxation occurred in tests conducted on the stress plateau and resulted in stable mean stress and stress amplitude responses that were comparable across the entire stress plateau despite the vast differences in strain.
2. The beneficial effect of tensile mean strain is a result of the stress-strain behavior of superelastic NiTi during phase transformation. The change in microstructure occurs with minimal stress increase accompanied by improvements in fatigue resistance from higher martensite volume fractions.
3. Higher volume fractions of martensite in NiTi specimens may increase the amount of mean stress relaxation that occurs in testing, up to a limit.
4. An energy model from the literature for mean stress/strain correction was implemented that accurately accounted for the unique fatigue behavior of superelastic NiTi under tensile mean strains.

CHAPTER VI

FUTURE WORK RECOMMENDATIONS

In light of the research findings in this work there are still many aspects of NiTi fatigue we don't fully understand. That said, here are some recommendations of future research that can fill in some of the current research gaps. A thorough comprehensive study of the fatigue behavior of superelastic NiTi in the presence of mean strains accompanied with in-situ microstructure monitoring. This data would provide helpful insight into linking fatigue behavior to microstructure in a robust quantified way. The novel data of interest would be average volume fraction of martensite, phase transformation front motion, and A ↔ M transformation amplitude. Additionally, research of fatigue behavior of specimens tested at larger ε_m's into the martensitic linear elastic region of the stress-strain response. This data could provide more understanding into stress-induced martensite behavior as well as an upper bound to the beneficial effects of ε_m.

REFERENCES

Allie, D.E., Herbert, C.J., and Walker, C.M. Nitinol stent fractures in the SFA. Endovasc Today 22–34.

ASTM, E.-96 (2004). Standard Test Methods for Determining Average Grain Size. In ASTM International, p.

Bahia, M.G.A., and Buono, V.T.L. (2005). Decrease in the fatigue resistance of nickel-titanium rotary instruments after clinical use in curved root canals. Oral Surgery, Oral Medicine, Oral Pathology, Oral Radiology, and Endodontology *100*, 249–255.

Benafan, O., Noebe, R.D., Padula II, S.A., Brown, D.W., Vogel, S., and Vaidyanathan, R. (2014). Thermomechanical cycling of a NiTi shape memory alloy-macroscopic response and microstructural evolution. International Journal of Plasticity *56*, 99–118.

Brinson, L.C., Schmidt, I., and Lammering, R. (2004). Stress-induced transformation behavior of a polycrystalline NiTi shape memory alloy: micro and macromechanical investigations via in situ optical microscopy. Journal of the Mechanics and Physics of Solids *52*, 1549–1571.

Buehler, W.J., Gilfrich, J.V., and Wiley, R.C. (1963). Effect of Low-Temperature Phase Changes on the Mechanical Properties of Alloys near Composition TiNi. Journal of Applied Physics *34*, 1475–1477.

Casati, R., Passaretti, F., and Tuissi, A. (2011). Effect of electrical heating conditions on functional fatigue of thin NiTi wire for shape memory actuators. Procedia Engineering *10*, 3423–3428.

Chan, K.S. (2010). Roles of microstructure in fatigue crack initiation. International Journal of Fatigue *32*, 1428–1447.

Condorelli, G.G., Bonaccorso, A., Smecca, E., Schäfer, E., Cantatore, G., and Tripi, T.R. (2010). Improvement of the fatigue resistance of NiTi endodontic files by surface and bulk modifications. International Endodontic Journal *43*, 866–873.

Delville, R., Malard, B., Pilch, J., Sittner, P., and Schryvers, D. (2011). Transmission electron microscopy investigation of dislocation slip during superelastic cycling of Ni–Ti wires. International Journal of Plasticity *27*, 282–297.

DesRoches, R., McCormick, J., and Delemont, M. (2004). Cyclic Properties of Superelastic Shape Memory Alloy Wires and Bars. Journal of Structural Engineering *130*, 38–46.

Dieter, G. (1961). Mechanical Metallurgy (McGraw-Hill Book Company).

Duerig, T., Pelton, A., and Stöckel, D. (1999). An overview of nitinol medical applications. Materials Science and Engineering: A *273–275*, 149–160.

Duerig, T.W., Melton, K.N., and Stöckel, D. (2013). Engineering Aspects of Shape Memory Alloys (Butterworth-Heinemann).

Eggeler, G., Hornbogen, E., Yawny, A., Heckmann, A., and Wagner, M. (2004). Structural and functional fatigue of NiTi shape memory alloys. Materials Science and Engineering: A *378*, 24–33.

Elahinia, M. (2015). Shape Memory Alloy Actuators: Design, Fabrication and Experimental Evaluation (John Wiley & Sons).

Elahinia, M.H., Hashemi, M., Tabesh, M., and Bhaduri, S.B. (2012). Manufacturing and processing of NiTi implants: A review. Progress in Materials Science *57*, 911–946.

Frick, C.P., Ortega, A.M., Tyber, J., Maksound, A.E.M., Maier, H.J., Liu, Y., and Gall, K. (2005). Thermal processing of polycrystalline NiTi shape memory alloys. Materials Science and Engineering: A *405*, 34–49.

Frotscher, M., Nörtershäuser, P., Somsen, C., Neuking, K., Böckmann, R., and Eggeler, G. (2009). Microstructure and structural fatigue of ultra-fine grained NiTi-stents. Materials Science and Engineering: A *503*, 96–98.

Frotscher, M., Wu, S., Simon, T., Somsen, C., Dlouhy, A., and Eggeler, G. (2011). Elementary Deformation and Damage Mechanisms During Fatigue of Pseudoelastic NiTi Microstents. Adv. Eng. Mater. *13*, B181–B186.

Fumagalli, L., Butera, F., and Coda, A. (2009). SmartFlex® NiTi Wires for Shape Memory Actuators. J. of Materi Eng and Perform *18*, 691–695.

Gall, K., Sehitoglu, H., Chumlyakov, Y.I., and Kireeva, I.V. (1999a). Tension–compression asymmetry of the stress–strain response in aged single crystal and polycrystalline NiTi. Acta Materialia *47*, 1203–1217.

Gall, K., Sehitoglu, H., Chumlyakov, Y.I., Kireeva, I.V., and Maier, H.J. (1999b). The Influence of Aging on Critical Transformation Stress Levels and Martensite Start Temperatures in NiTi: Part II—Discussion of Experimental Results. J. Eng. Mater. Technol *121*, 28–37.

Gall, K., Yang, N., Sehitoglu, H., and Chumlyakov, Y.I. (2001). Fracture of precipitated NiTi shape memory alloys. International Journal of Fracture *109*, 189–207.

Gall, K., Dunn, M.L., Liu, Y., Labossiere, P., Sehitoglu, H., and Chumlyakov, Y.I. (2002). Micro and Macro Deformation of Single Crystal NiTi. J. Eng. Mater. Technol *124*, 238–245.

Gall, K., Tyber, J., Wilkesanders, G., Robertson, S.W., Ritchie, R.O., and Maier, H.J. (2008). Effect of microstructure on the fatigue of hot-rolled and cold-drawn NiTi shape memory alloys. Materials Science and Engineering: A *486*, 389–403.

Gloanec, A.-L., Cerracchio, P., Reynier, B., Van Herpen, A., and Riberty, P. (2010). Fatigue crack initiation and propagation of a TiNi shape memory alloy. Scripta Materialia *62*, 786–789.

Gollerthan, S., Young, M.L., Baruj, A., Frenzel, J., Schmahl, W.W., and Eggeler, G. (2009). Fracture mechanics and microstructure in NiTi shape memory alloys. Acta Materialia *57*, 1015–1025.

He, X., Zhao, L., Wang, X., Zhang, R., and Li, M. (2006). Transformation behaviour with thermal cycling in Ti50Ni43Cu7 shape memory alloy. Materials Science and Engineering: A *427*, 327–330.

Holtz, R.L., Sadananda, K., and Imam, M.A. (1999). Fatigue thresholds of Ni-Ti alloy near the shape memory transition temperature. International Journal of Fatigue *21*, *Supplement 1*, S137–S145.

Iadicola, M.A., and Shaw, J.A. (2002). The Effect of Uniaxial Cyclic Deformation on the Evolution of Phase Transformation Fronts in Pseudoelastic NiTi Wire. Journal of Intelligent Material Systems and Structures *13*, 143–155.

James, B., Foulds, J., and Eiselstein, L. (2005). Failure analysis of NiTi wires used in medical applications. J Fail. Anal. and Preven. *5*, 82–87.

Kang, G., Kan, Q., Yu, C., Song, D., and Liu, Y. (2012). Whole-life transformation ratchetting and fatigue of super-elastic NiTi Alloy under uniaxial stress-controlled cyclic loading. Materials Science and Engineering: A *535*, 228–234.

Kauffman, G.B., and Mayo, I. (1997). The Story of Nitinol: The Serendipitous Discovery of the Memory Metal and Its Applications. Chem. Educator *2*, 1–21.

Kim, Y. (2002). Fatigue Properties of the Ti-Ni Base Shape Memory Alloy Wire. Materials Transactions *43*, 1703–1706.

Lagoudas, D.C., Miller, D.A., Rong, L., and Kumar, P.K. (2009). Thermomechanical fatigue of shape memory alloys. Smart Mater. Struct. *18*, 085021.

Leo, D.J., Weddle, C., Naganathan, G., and Buckley, S.J. (1998). Vehicular applications of smart material systems. pp. 106–116.

Mahtabi, M., and Shamsaei, N. (2017). A Cumulative Energy-Based Model for Fatigue Behavior of Superelastic NiTi Considering Cyclic Deformation and Mean Strain and Stress Effects.

Mahtabi, M.J., and Shamsaei, N. (2016). A modified energy-based approach for fatigue life prediction of superelastic NiTi in presence of tensile mean strain and stress. International Journal of Mechanical Sciences *117*, 321–333.

Mahtabi, M.J., Shamsaei, N., and Mitchell, M.R. (2015a). Fatigue of Nitinol: The state-of-the-art and ongoing challenges. Journal of the Mechanical Behavior of Biomedical Materials *50*, 228–254.

Mahtabi, M.J., Shamsaei, N., and Rutherford, B. (2015b). Mean Strain Effects on the Fatigue Behavior of Superelastic Nitinol Alloys: An Experimental Investigation. Procedia Engineering *133*, 646–654.

Maletta, C., Sgambitterra, E., Furgiuele, F., Casati, R., and Tuissi, A. (2012). Fatigue of pseudoelastic NiTi within the stress-induced transformation regime: a modified Coffin–Manson approach. Smart Mater. Struct. *21*, 112001.

Mao, S., Han, X., Wu, M.H., Zhang, Z., Hao, F., Liu, D., Zhang, Y., and Hou, B. (2006). Effect of Cyclic Loading on Apparent Young's Modulus and Critical Stress in Nano-Subgrained Superelastic NiTi Shape Memory Alloys. Materials Transactions *47*, 735–741.

McKelvey, A.L., and Ritchie, R.O. (2001). Fatigue-crack growth behavior in the superelastic and shape-memory alloy nitinol. Metall and Mat Trans A *32*, 731–743.

Melton, K.N., and Mercier, O. (1979b). Fatigue of NITI thermoelastic martensites. Acta Metallurgica *27*, 137–144.

Melton, K.N., and Mercier, O. (1979a). The effect of the martensitic phase transformation on the low cycle fatigue behaviour of polycrystalline Ni□Ti and Cu□Zn□Al alloys. Materials Science and Engineering *40*, 81–87.

Mertmann, M., and Vergani, G. (2008). Design and application of shape memory actuators. Eur. Phys. J. Spec. Top. *158*, 221–230.

Michal, G.M., and Sinclair, R. (1981). The structure of TiNi martensite. Acta Cryst B, Acta Cryst Sect B, Acta Crystallogr B, Acta Crystallogr Sect B, Acta Crystallogr B Struct Crystallogr Cryst Chem, Acta Crystallogr Sect B Struct Crystallogr Cryst Chem *37*, 1803–1807.

Miyazaki, S., Imai, T., Igo, Y., and Otsuka, K. (1986). Effect of cyclic deformation on the pseudoelasticity characteristics of Ti-Ni alloys. MTA *17*, 115–120.

Miyazaki, S., Mizukoshi, K., Ueki, T., Sakuma, T., and Liu, Y. (1999). Fatigue life of Ti–50 at.% Ni and Ti–40Ni–10Cu (at.%) shape memory alloy wires. Materials Science and Engineering: A *273–275*, 658–663.

Mohd Jani, J., Leary, M., Subic, A., and Gibson, M.A. (2014). A review of shape memory alloy research, applications and opportunities. Materials & Design (1980-2015) *56*, 1078–1113.

Morgan, N.B., Painter, J., and Moffat, A. (2004). Mean Strain Effects and Microstructural Observations During in vitro Fatigue Testing of NiTi. In Proceedings of the International Conference on Shape Memory and Superelastic Technologies, (ASM International), pp. 303–310.

Moumni, Z., Herpen, A.V., and Riberty, P. (2005). Fatigue analysis of shape memory alloys: energy approach. Smart Mater. Struct. *14*, S287.

Moumni, Z., Zaki, W., and Maitournam, H. (2009). Cyclic behavior and energy approach to the fatigue of shape memory alloys. Journal of Mechanics of Materials and Structures *4*, 395–411.

Nikanorov, A., Smouse, H.B., Osman, K., Bialas, M., Shrivastava, S., and Schwartz, L.B. (2008). Fracture of self-expanding nitinol stents stressed in vitro under simulated intravascular conditions. Journal of Vascular Surgery *48*, 435–440.

Norfleet, D.M., Sarosi, P.M., Manchiraju, S., Wagner, M.F.-X., Uchic, M.D., Anderson, P.M., and Mills, M.J. (2009). Transformation-induced plasticity during pseudoelastic deformation in Ni–Ti microcrystals. Acta Materialia *57*, 3549–3561.

Otsuka, K., and Ren, X. (2005). Physical metallurgy of Ti–Ni-based shape memory alloys. Progress in Materials Science *50*, 511–678.

Paradis, A., Terriault, P., Brailovski, V., and Torra, V. (2008). On the partial recovery of residual strain accumulated during an interrupted cyclic loading of NiTi shape memory alloys. Smart Mater. Struct. *17*, 065027.

Patel, M.M., Mitchell, M.R., Jerina, K., and Dean, S.W. (2007). Characterizing Fatigue Response of Nickel-Titanium Alloys by Rotary Beam Testing. Journal of ASTM International *4*, 100390.

Pelton, A.R. (2011). Nitinol Fatigue: A Review of Microstructures and Mechanisms. J. of Materi Eng and Perform *20*, 613–617.

Pelton, A.R., Dicello, J., and Miyazaki, S. (2000). Optimisation of processing and properties of medical grade Nitinol wire. Minimally Invasive Therapy & Allied Technologies *9*, 107–118.

Pelton, A.R., Gong, X.-Y., and Duerig, T. (2003). Fatigue Testing of Diamond-Shaped Specimens. In Medical Device Materials: Proceedings of the Materials and Processes for Medical Devices Conference, pp. 199–204.

Pelton, A.R., Duerig, T.W., and Stöckel, D. (2004). A guide to shape memory and superelasticity in Nitinol medical devices. Minimally Invasive Therapy & Allied Technologies *13*, 218–221.

Pelton, A.R., Schroeder, V., Mitchell, M.R., Gong, X.-Y., Barney, M., and Robertson, S.W. (2008). Fatigue and durability of Nitinol stents. Journal of the Mechanical Behavior of Biomedical Materials *1*, 153–164.

Pelton, A.R., Fino-Decker, J., Vien, L., Bonsignore, C., Saffari, P., Launey, M., and Mitchell, M.R. (2013). Rotary-bending fatigue characteristics of medical-grade Nitinol wire. Journal of the Mechanical Behavior of Biomedical Materials *27*, 19–32.

Predki, W., Klönne, M., and Knopik, A. (2006). Cyclic torsional loading of pseudoelastic NiTi shape memory alloys: Damping and fatigue failure. Materials Science and Engineering: A *417*, 182–189.

Reyes-Mena, A., Jensen, C., Bard, E., Turner, D.C., Erdmann, K.G., Qui, Q., Gao, B., Lu, J., and Zhou, O. (2005). International Centre for Diffraction Data 2005. Advances in X-Ray Analysis *48*, 204209.

Robertson, S.W., and Ritchie, R.O. (2007). In vitro fatigue–crack growth and fracture toughness behavior of thin-walled superelastic Nitinol tube for endovascular stents: A basis for defining the effect of crack-like defects. Biomaterials *28*, 700–709.

Robertson, S.W., Pelton, A.R., and Ritchie, R.O. (2012). Mechanical fatigue and fracture of Nitinol. International Materials Reviews *57*, 1–37.

Runciman, A., Xu, D., Pelton, A.R., and Ritchie, R.O. (2011). An equivalent strain/Coffin–Manson approach to multiaxial fatigue and life prediction in superelastic Nitinol medical devices. Biomaterials *32*, 4987–4993.

Sawaguchi, T.A., Kausträter, G., Yawny, A., Wagner, M., and Eggeler, G. (2003). Crack initiation and propagation in 50.9 at. pct Ni-Ti pseudoelastic shape-memory wires in bending-rotation fatigue. Metall and Mat Trans A *34*, 2847–2860.

Schneider, C., Rasband, W., and Eliceiri, K. (2012). NIH Image to ImageJ: 25 years of image analysis - ProQuest. Nature Methods.

Scirè Mammano, G., and Dragoni, E. (2014). Functional fatigue of Ni–Ti shape memory wires under various loading conditions. International Journal of Fatigue *69*, 71–83.

Sehitoglu, H., Anderson, R., Karaman, I., Gall, K., and Chumlyakov, Y. (2001). Cyclic deformation behavior of single crystal NiTi. Materials Science and Engineering: A *314*, 67–74.

Shabalovskaya, S.A. (1996). On the nature of the biocompatibility and on medical applications of NiTi shape memory and superelastic alloys. Bio-Medical Materials and Engineering *6*, 267–289.

Shayesteh Moghaddam, N., Jahadakbar, A., Amerinatanzi, A., Elahinia, M., Miller, M., and Dean, D. (2016). Metallic Fixation of Mandibular Segmental Defects: Graft Immobilization and Orofacial Functional Maintenance. Plast Reconstr Surg Glob Open *4*.

Smith, W., and Hashemi, J. (2006). Foundations of materials science and engineering (McGraw-Hill Book Company).

Song, G., Ma, N., and Li, H.-N. (2006). Applications of shape memory alloys in civil structures. Engineering Structures *28*, 1266–1274.

Stephens, R.I., Fatemi, A., Stephens, R.R., and Fuchs, H.O. (2000). Metal Fatigue in Engineering (John Wiley & Sons).

Tabanli, R.M., Simha, N.K., and Berg, B.T. (1999). Mean stress effects on fatigue of NiTi. Materials Science and Engineering: A *273–275*, 644–648.

Tabanli, R.M., Simha, N.K., and Berg, B.T. (2001). Mean strain effects on the fatigue properties of superelastic NiTi. Metall and Mat Trans A *32*, 1866–1869.

Tobushi, H., Hachisuka, T., Yamada, S., and Lin, P.-H. (1997). Rotating-bending fatigue of a TiNi shape-memory alloy wire. Mechanics of Materials *26*, 35–42.

Tobushi, H., Hachisuka, T., Hashimoto, T., and Yamada, S. (1998). Cyclic deformation and fatigue of a TiNi shape-memory alloy wire subjected to rotating bending. Journal of Engineering Materials and Technology *120*, 64–70.

Tolomeo, D., Davidson, S., and Santinoranont, M. (2000). Cyclic Properties of Superelastic Nitinol: Design Implications. In SMST: Proceedings of the International Conference on Shape Memory and Superelastic Technologies., pp. 471–476.

Urbina, C., De la Flor, S., and Ferrando, F. (2009). Effect of thermal cycling on the thermomechanical behaviour of NiTi shape memory alloys. Materials Science and Engineering: A *501*, 197–206.

Vaidyanathan, R., Dunand, D.C., and Ramamurty, U. (2000). Fatigue crack-growth in shape-memory NiTi and NiTi–TiC composites. Materials Science and Engineering: A *289*, 208–216.

APPENDIX A

SUPPLEMENTAL DATA

This appendix includes stress-strain data gathered during testing that was not included in the main body of this work. There is an incomplete data set for ε_a = 0.3% as well as figures for the ε_a = 0.3% and 0.4% that show agreement with the data provided in the main body.

Table 7 Fatigue data for all tests including the incomplete ε_a = 0.3% data set

ε_a (%)	ε_m (%)	R_ε	N_f (Cycles)	σ_a (MPa)	σ_m (MPa)	R_σ	E_A (GPa)	Total Mean Stress Relaxation (MPa)
0.4	0.40	0.00	29,696	199.40	264.16	0.14	64.5	-90.84
0.4	0.80	0.33	12,346	145.85	391.55	0.46	70.3	20.36
0.4	2.20	0.69	9,051	73.59	559.42	0.77	70.2	42.93
0.4	3.80	0.81	10,603	82.75	537.56	0.73	67.7	102.31
0.3	2.20	0.76	16,909	74.35	548.16	0.76	68.4	57.61
0.3	3.80	0.85	19,745	64.08	543.41	0.79	71.7	117.77
0.2	0.27	0.14	153,467	112.52	294.86	0.45	76.1	-96.28
0.2	0.53	0.45	71,321	83.94	421.04	0.67	75.3	-51.66
0.2	1.47	0.76	23,355	45.50	546.30	0.85	66.3	58.54
0.2	2.53	0.85	78,069	48.45	524.47	0.83	73.2	89.36
0.2	3.80	0.90	201,826	48.75	526.41	0.83	74.2	133.98

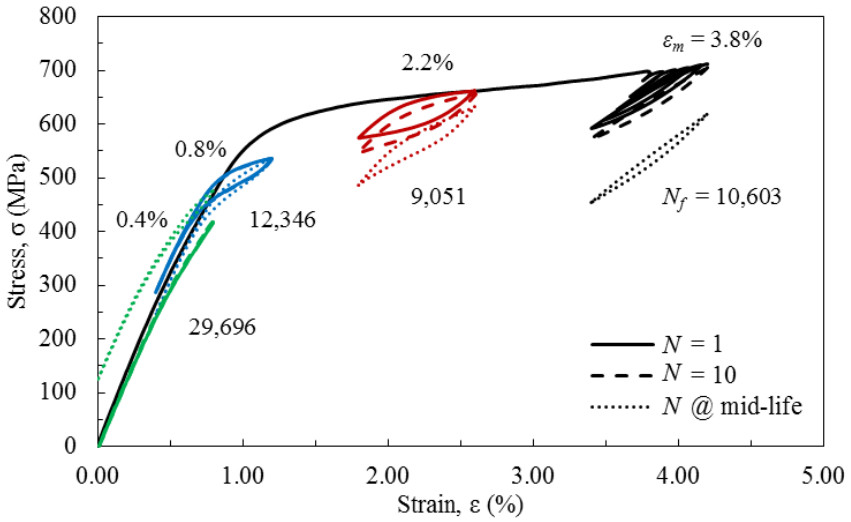

Figure 23 The hysteresis loops for ε_a = 0.4% and ε_m = 0.4% (purple), 0.8% (green), 2.2% (blue), and 3.80% (black) for the first cycle (solid line), tenth cycle (dashed line), and stable cycle (dotted)

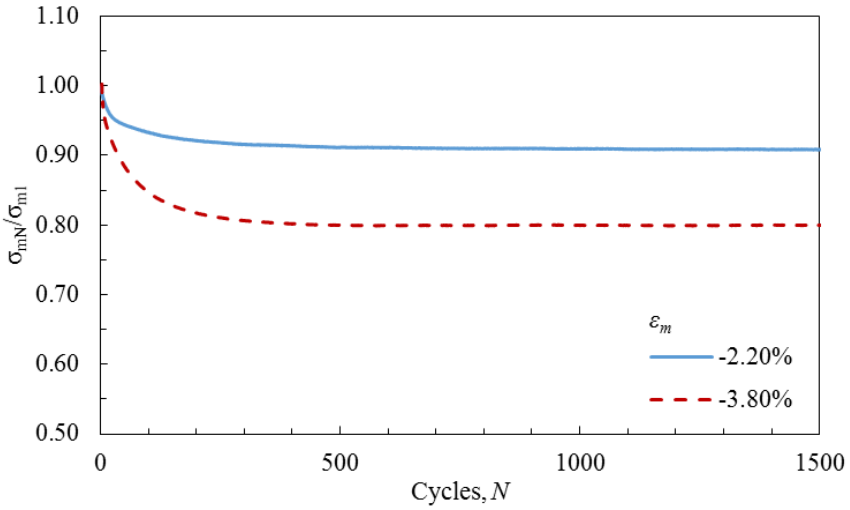

Figure 24 Evolution of mean stress relaxation at different mean strain levels for ε_a = 0.4%

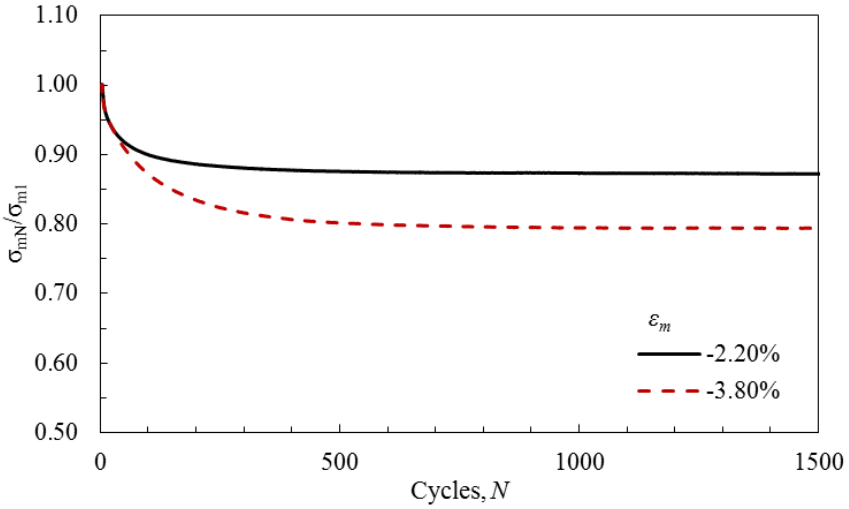

Figure 25 Evolution of mean stress relaxation at different mean strain levels for ε_a = 0.3%

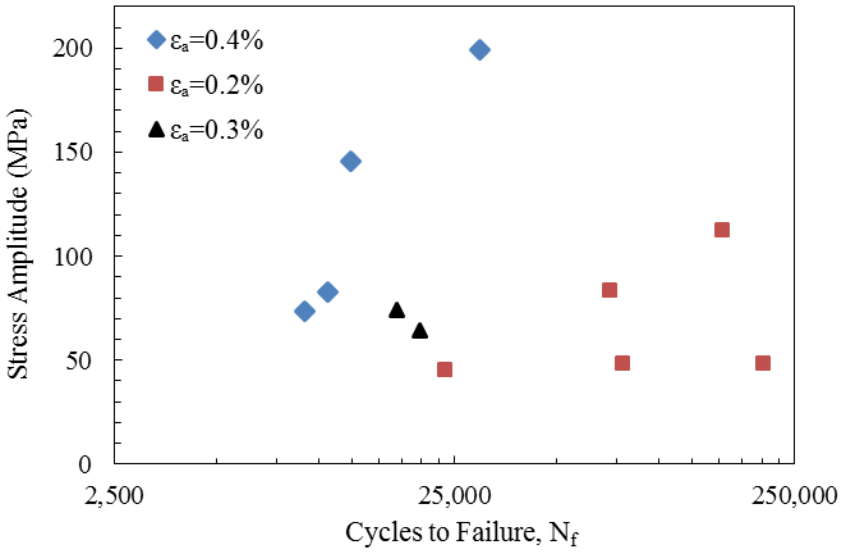

Figure 26 Figure 16 with the ε_a = 0.3% data included

Table 8 Figure 3 with the ε_a = 0.3% data included

ε_a (%)	ε_m (%)	Relaxation to Stable Response (MPa)	Relaxation Rate (MPa/cycle)	Relaxation at Failure
0.2	1.47	58.54	0.05	58.5
0.2	2.53	96.35	0.08	96.4
0.2	3.80	123.94	0.11	134.0
0.3	2.20	69.58	0.07	69.6
0.3	3.80	116.79	0.11	117.8
0.4	2.20	42.93	0.04	42.9
0.4	3.80	99.78	0.10	102.3

Table 9 Table 4 with the ε_a = 0.3% data included

Austenitic Linear Elastic Range			Phase Transformation Range		
ε_a (%)	ε_m (%)	σ_a (MPa)	ε_a (%)	ε_m (%)	σ_a (MPa)
0.2	0.27	112.52	0.2	1.47	45.50
0.2	0.53	83.94	0.2	2.53	48.45
			0.2	3.80	48.75
			0.3	2.20	74.35
			0.3	3.80	64.08
0.4	0.4	199.40	0.4	2.20	73.59
0.4	0.8	145.85	0.4	3.80	82.75
Average		135.43 ± 42.94	Average		62.49 ± 13.90